Tectonics, gold structural control and lithostratigraphy of Ferkessédougou metasedimentary basin, northern Côte d'Ivoire.

Yaya Zana OUATTARA[1] and GBELE OUATTARA[2]

[1]Institut National Polytechnique Félix HOUPHOUET-BOIGNY (INP-HB)
[2]Institut National Polytechnique Félix Houphouët-Boigny

November 23, 2022

Abstract

The study area is located in the Ferkessédougou belt in northern Côte d'Ivoire, precisely 30 km east of the city of Ferkessédougou. The aim of this study is to understand the tectonic which control gold mineralization. A combination of remote analysis and field mapping work, trenching, reverse circulation drilling hole, core drilling hole was carried out and finally laboratory work (microscopy). Different processing such as ACP, adaptive filters have been applied to Landsat 8 and Radarsat satellite images, in order to enhance information for better lineament extraction. Also, different complementary techniques (horizontal gradient, Euler deconvolution) were applied to the areomagnetic map in order to highlight the different lineaments.

Four sets of lineaments have been producted by these images: N080-N100, N030-050, N000-N020, N120-N135.The validation of these different linear structures was made with field data. Thus, in the field, the metasediments show a strong S1 schistosity, stirikes NNE, with and dips towards the South-East, compatible with a D1 shortening episode. The emplacement of leucogranitic batholith and tonalite induces deformation (D2) which is shearing foliation S2.). Later, diorite dykes induces the S3 shearing foliation. The earliest form of gold mineralization is located in quartz veins and fractures filled by sulphide (pyrite). The second form of gold mineralization is disseminated and hosted in the sheared contacts betwween intrusive units with the metasediments. Studies show that quartz veins control the highest gold grades in tonalite unit. The mineralization of our study area is an IRGS type.

Keywords: Gold, mineralization, Pyrite, Ferkessedougou, Ivory Coast.

Introduction

The significant West Africa's gold production hosted by Birimian's rocks (Milesi et al., 1989). In addition, gold production in recent years located in the Paleoproterozoic domain is the strongest growth in the world (Masurel, 2015). Seventeen Birimian belt are distributed over two reference alignments, Tehini-Dimbokro in the East and Ferkessedougou - Soubré in the center have been identified in Côte d'Ivoire (Tagini, 1971; Yace, 2002). Our study area is located thirty (30) km eastern of the town of Ferkessedougou, in northern Côte d'Ivoire and situated in the belt of Ferkessédougou which is subject of exploration and artisanal mining. This belt has been identified as a gold region in the geostructural classification gold-bearing regions of Côte d'Ivoire (Sonnendrucker, 1969). This study will allow us to carry out the chronology of various deformations, as well as the model of gold mineralization in this area.

1. GEOLOGICAL CONTEXT

Ivory Coast is located in the southern part of the West African craton, precisely on the Man Ridge (Bessoles, 1977). It comprises two large unevenly distributed geological units which are, on the one hand, a narrow coastal sedimentary basin bordering the Gulf of Guinea in the south of the country and, on the other hand, a crystalline basement of Precambrian age which covers 97.5% of the national territory. The Pre-Ecambrian basement of Côte d'Ivoire is subdivided into two major domains depending on the age of the formations encountered, which are: (i) the Archean domain formed of crystalline and crystallophyllian rocks and (ii) the Paleoproterozoic domain formed of rocks crystalline and meta - volcano -sedimentary (Figure 1) (Bessoles, 1977). These two domains of unequal areas are separated by the Sassandra fault with sinistral movement oriented North-South. The Paleoproterozoic domain in which our study area is located was structured by the Eburnean megacycle. The formations of this domain in Côte d'Ivoire are volcano-sedimentary belt generally oriented NNE-SSW (Tagini, 1971; Daouda, 1998). On a regional scale, the study area is composed from west to east: of a biotite granite, metasediments namely: sandstones and argillites and finally a granodiorite to the west. The study area is composed from west to east: of a granite, volcanosediments and the sequence: argillites, pelites and shale (Figure 2) (WAXI, 2018). This granite located to the west of the study area is a vast and very extensive pluri-plutonic batholith (more than 500 km in length), it is an assembly of small two-mica plutons relatively similar in shape to laccoliths (Ouattara, 1998).

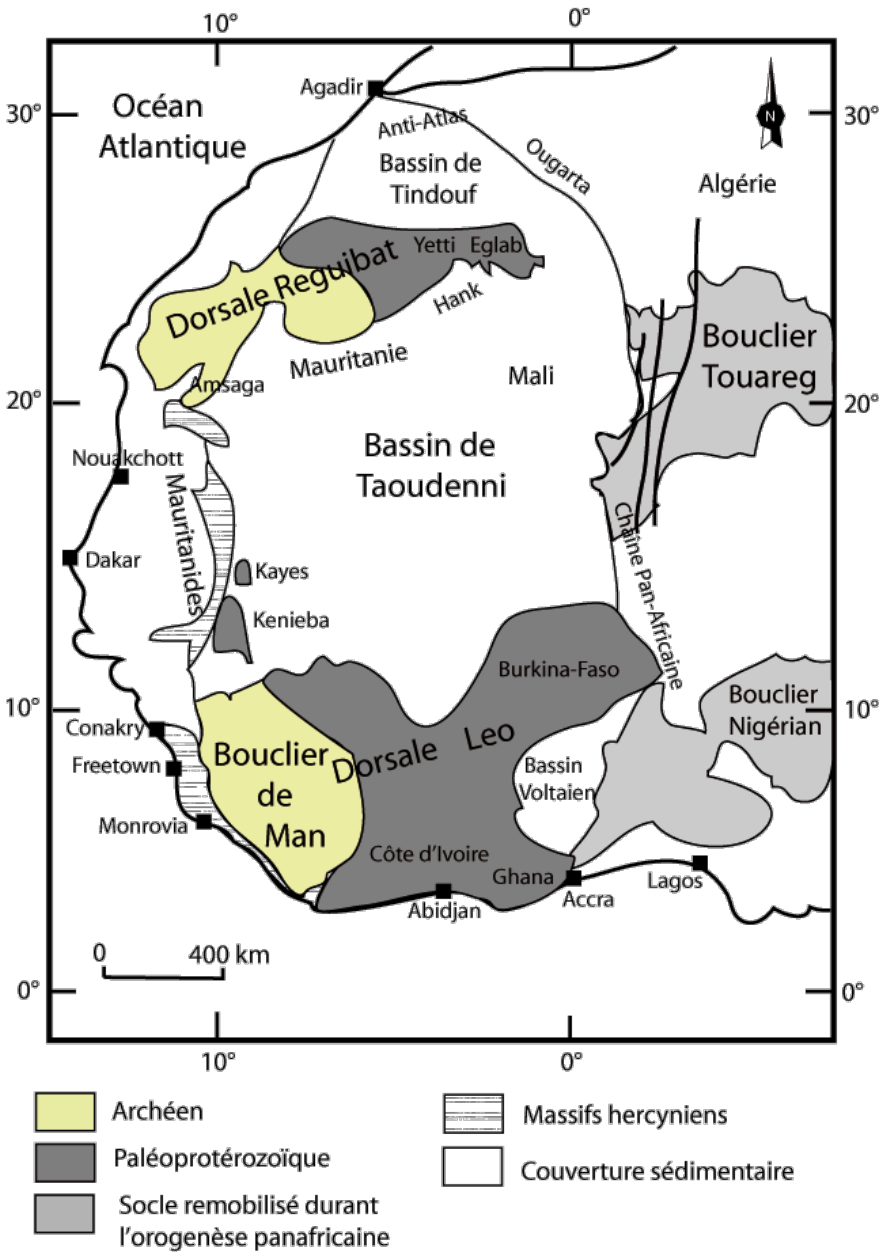

Figure 1: Shematic map of West Africa Craton (Boher et al., 1992)

Figure 2 . Presentation of the study area on geological map of WAXI (2018)

2. MATERIAL

The equipment used to carry out this work includes remote analysis data and field data. Remote analysis data includes satellite image Landsat 8 and the radarsat image. In addition to these images, there is the geological map of WAXI 2018. The images were downloaded and processed from softwares. These are Landsat 8 optical image, radarsat image of the study area. Satellite images Landsat 8 were downloaded from the website at http://www.earthexplorer.usgs.gov. According to Landsat image, we used a total of 11 images (bands 1, 2, 3, 4, 5, 6-1, 6, 7, 8, 9, 10 and 11). Aeromagnetic image has been treated also.The survey

was carried out by Kenting Earth Sciences Ltd, during the years 1974 and 1975 as part of a cooperation program between the Government of Canada and Côte d'Ivoire.The softwares used for image processing are Envi, Arc Gis, Google Earth Pro and Qgis, Geosoft. Structural data was processed with Global Mapper, Georient and Leapfrog softwares.

3. METHODS

Relative to the landsat 8 image, the band 8 has been choosen. The band 8 is the panchromatic band with a resolution of 15 meters on the ground. After atmospheric and radiometric corrections applied to band 8, Principal Composition Analysis (PCA) and various processing filters were applied to enhance the perception of linear structures. PCA is an effective technique which allows to accentuate multi-spectral images for fine geological interpretations (Biémi et al., 1991) because it allows to reduce the information contained in several bands, sometimes highly correlated (redundancy of spectral information) in a number more restricted of components. Component 1 (band 1 of PCA) was retained. Therefore, we have chosen to apply the filter to this first principal component. Filters have also been applied to the radarsat image. Filtering consists in changing the value of a pixel according to those of its neighbors (Touzi et al., 1988, Nezry, et al., 1991; Lopez, et al., 1992; Yésou, et al., 1993). We applied the four Sobel filters, the PREWITT filter and the YESOU filter to the two images. These directional filters whose application matrices make it possible to bring out or mask specific characteristics of an image based on their frequency related to texture (Himyari, et al., 2002; Jourda, et al., 2006; Ta, et al,. 2008; Djemai, et al., 2009; Guergour, et al., 2009; Kouamé, et al., 2009). Then, the flowchart of the processing carried out on the images is presented in figure 3. The lineament maps resulting from these images were obtained. Finally, we validated the Landsat image and the radarsat image using the field data and pre-existing maps. After extracting the study area from the raw aeromagnetic map, the processing consists of applying specific filters. We successively applied the horizontal and vertical derivatives and the magnitude of the horizontal gradient. The calculation of the Euler deconvolution, by applying the structural index "1", made it possible to highlight faults at depth and to follow their connection with the faults affecting the cover in accordance with the work of (Vanié and al., 2005, Vanié et and., 2006, El Gout et al., 2009, Khattach, 2010). The results of the various treatments are presented as lineament maps and rose diagram. (Vanié et al., 2006).

Figure 3.a Landsat8 Image processing flowchart; **b**Radarsat Image processing flowchart; **c** AeromagImage processing flowchart

During the differents geological mapping campaigns, the rare outcrops that appear in contact with the granite Ferkessedougou batholith and the metasediments, along the watercourses and finally along the tracks allowed us to identify several structural elements. Although some outcrops are not directly located on the mineralization, nevertheless they offer several east-west sections through the granite contact (Ferkessedougou batholith) and the metasediments. Also, it will be necessary to add the cartography of 7100m in length of thirty-seven (37) trenches during which nine hundred eighty-seven (987) structures were measured and one thousand nine hundred and sixty (1960) structures from nine (19) core drilling. The planar structures are bedding, shearing foliation, veins or sometimes quartz and carbonates veinlets. All of these data have been classified according to their nature and their chronological relationship, in to deformation structures D1, D2 and D3.

4. RESULTS

4.1 Images data

After image processing, lineament maps from Landsat 8, Radarsat and aeromagnetic images were obtained. The rose diagram were made from these lineament maps. The raw Landsat 8 image as well as the lineament map of the image are presented below (Figure 4 and 5). The radarsat image and its lineament map are presented below (Figure 6 and 7). the Aeromag image and its lineament map are presented below (Figure 8 and 9).

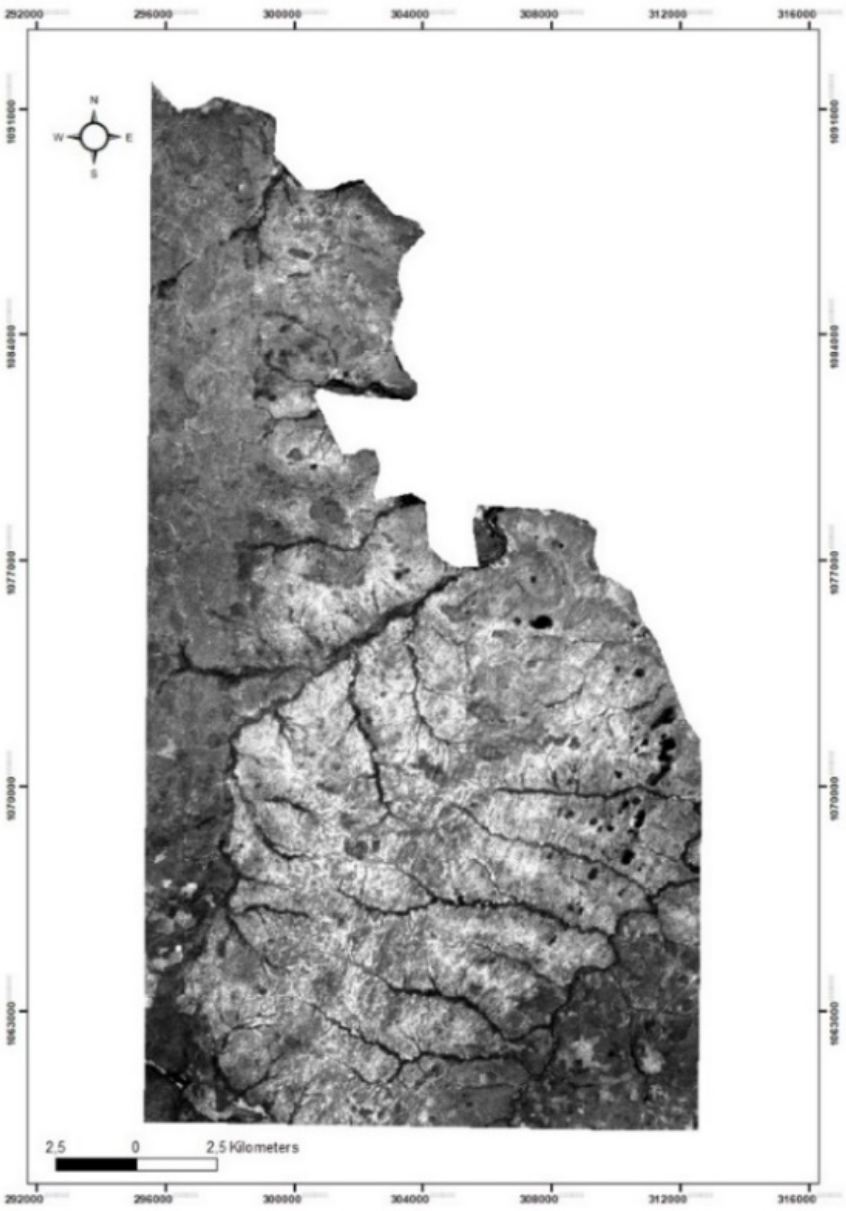

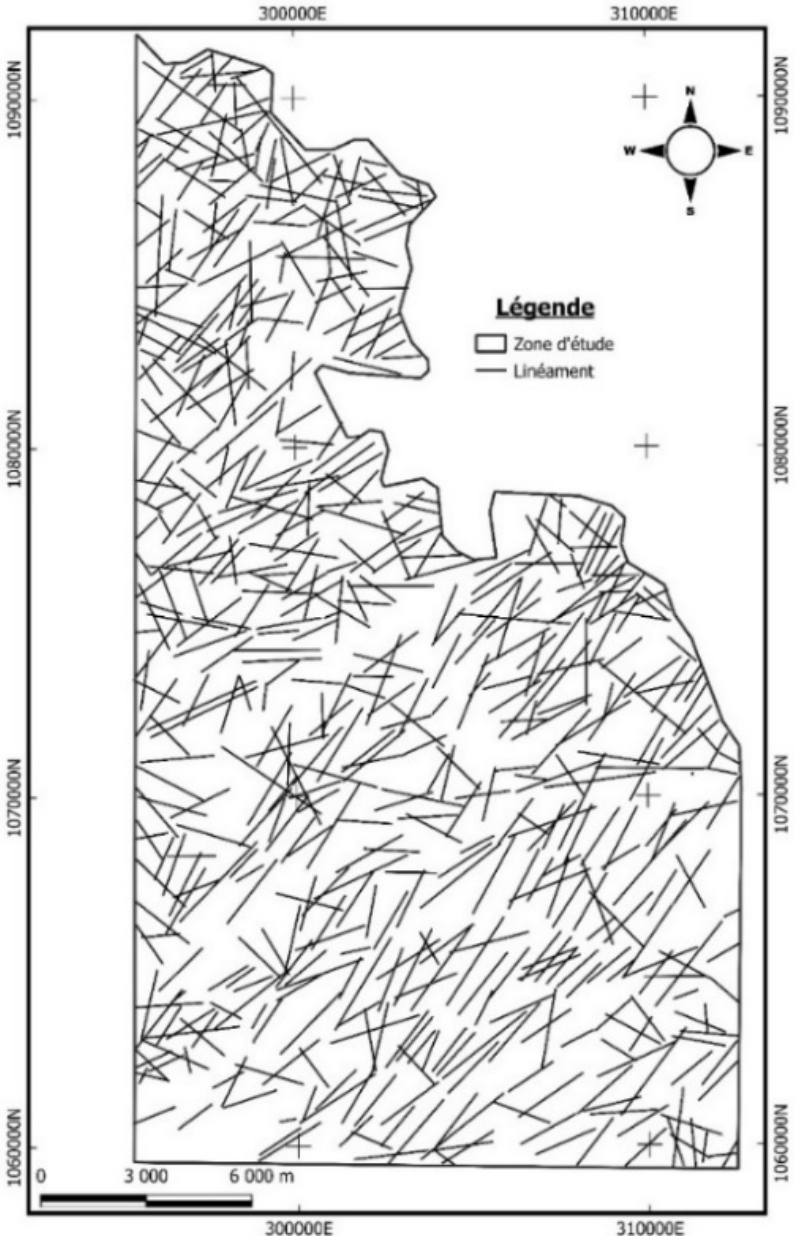

Figure 4. *Raw Landsat 8 image* ***Figure 5.****Lineament map from Landsat 8 image*

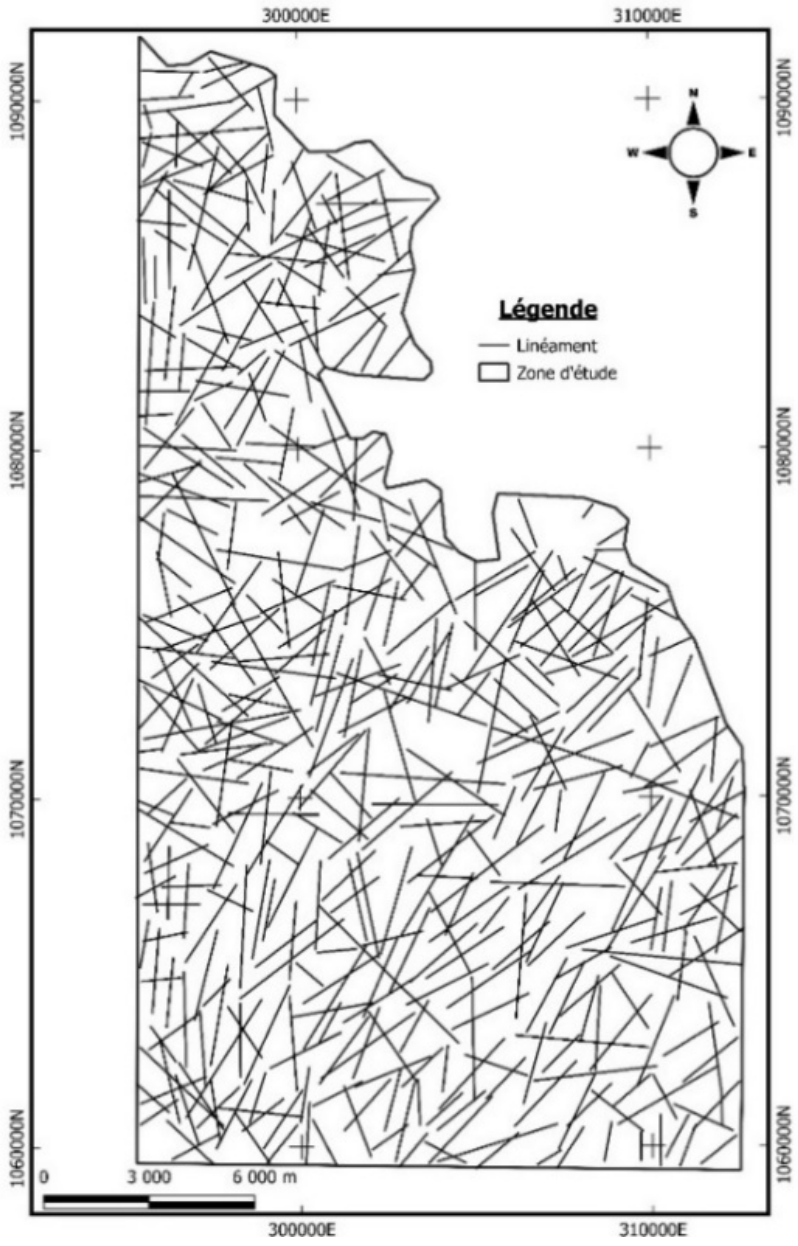

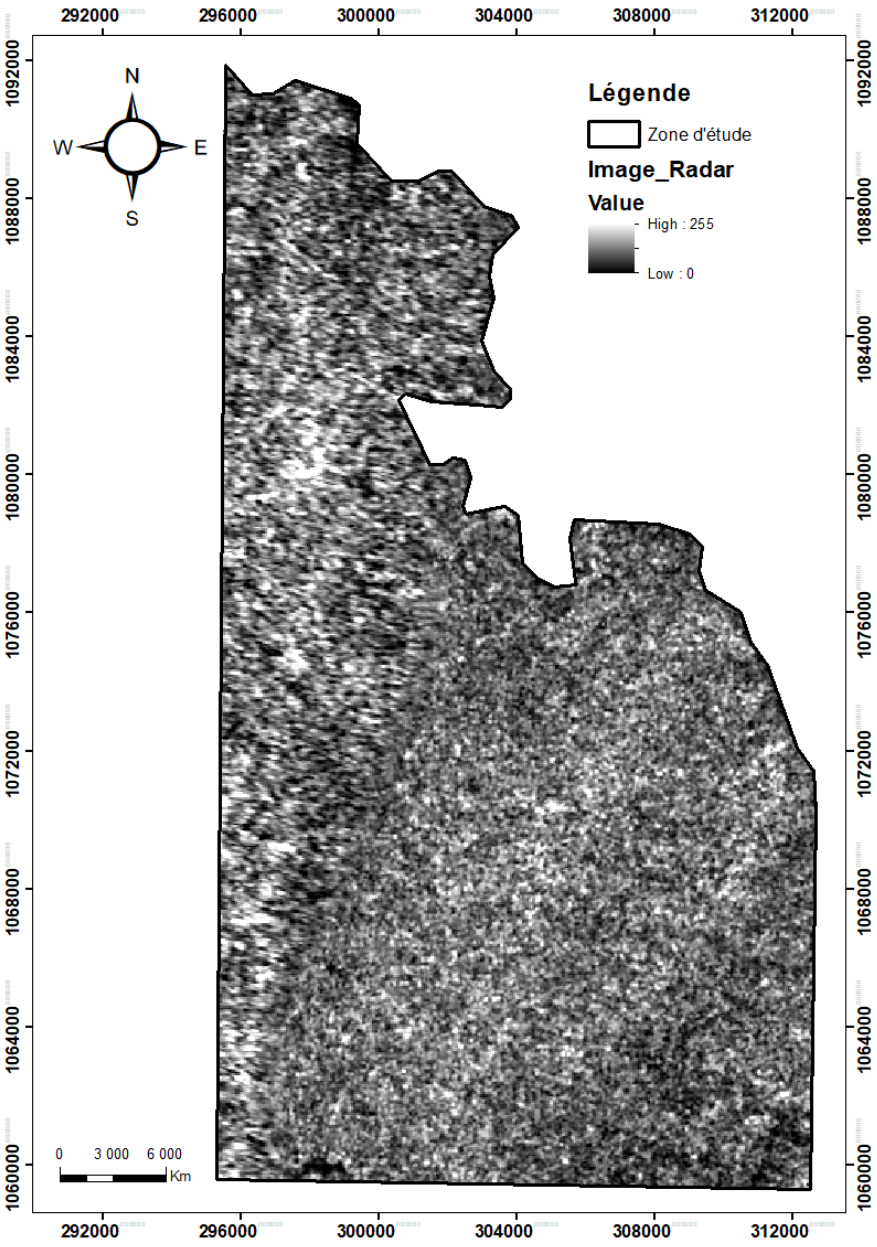

Figure 6. *Raw Radarsat image* ***Figure 7.*** *Lineament map from the radarsat image*

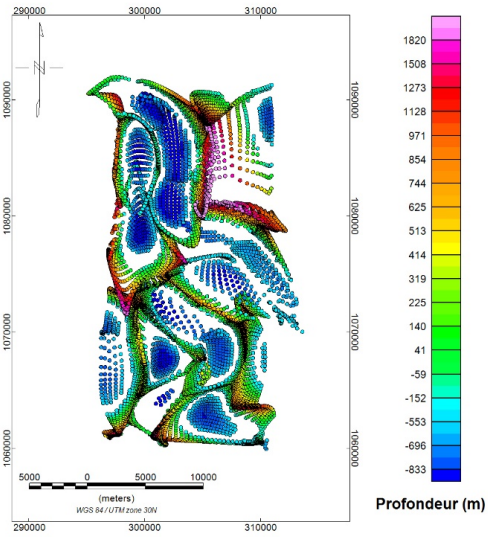

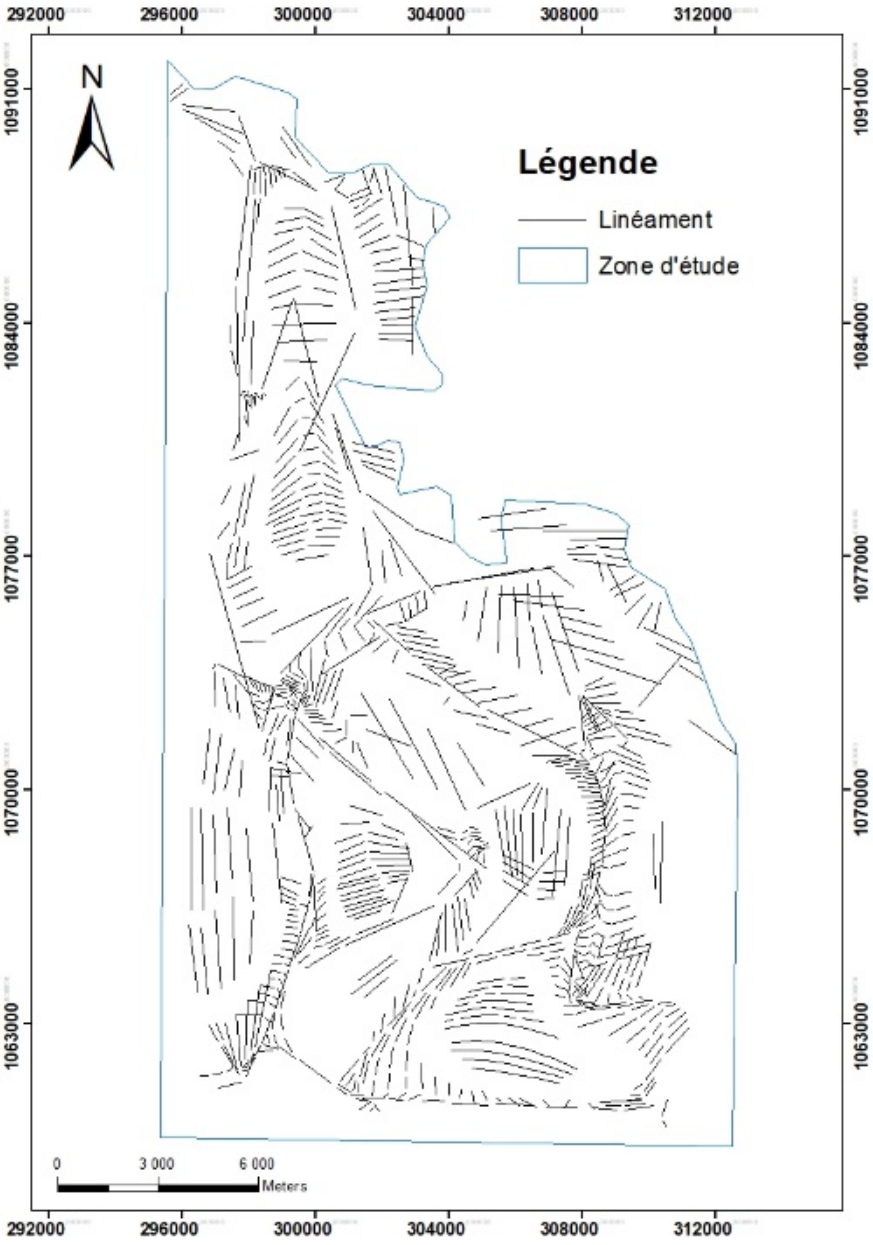

Figure 8. *Euler's solution map* ***Figure 9.****Lineament map from aeromagnetic image*

After the analysis of lineament maps from landsat 8 and radarsat, aeromagnetic images, the main directions of lineaments are presented as four sets namely N080-N100, N030-050, N000-N020, N120-N135. We will compare these results with field data (Figure 10).

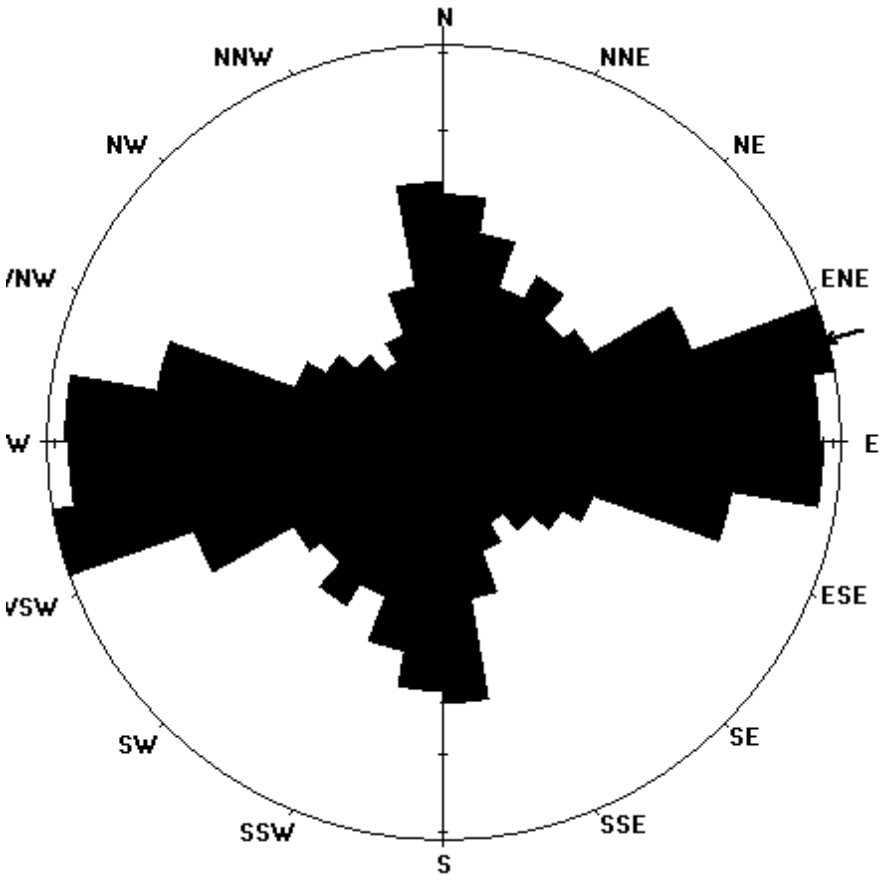

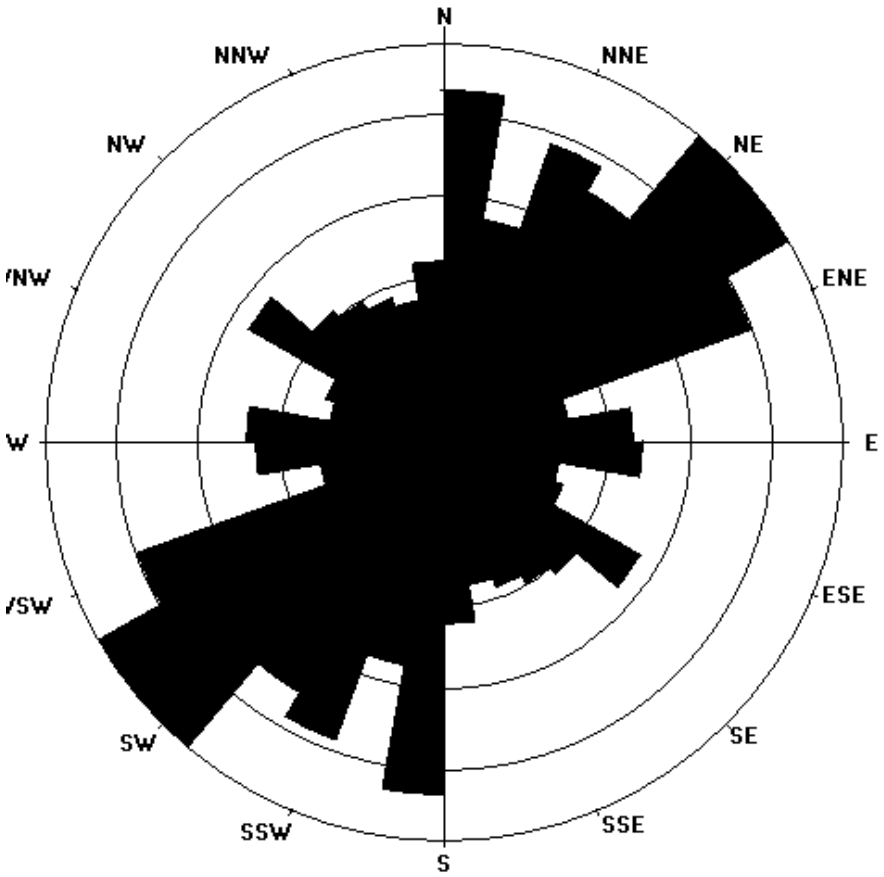

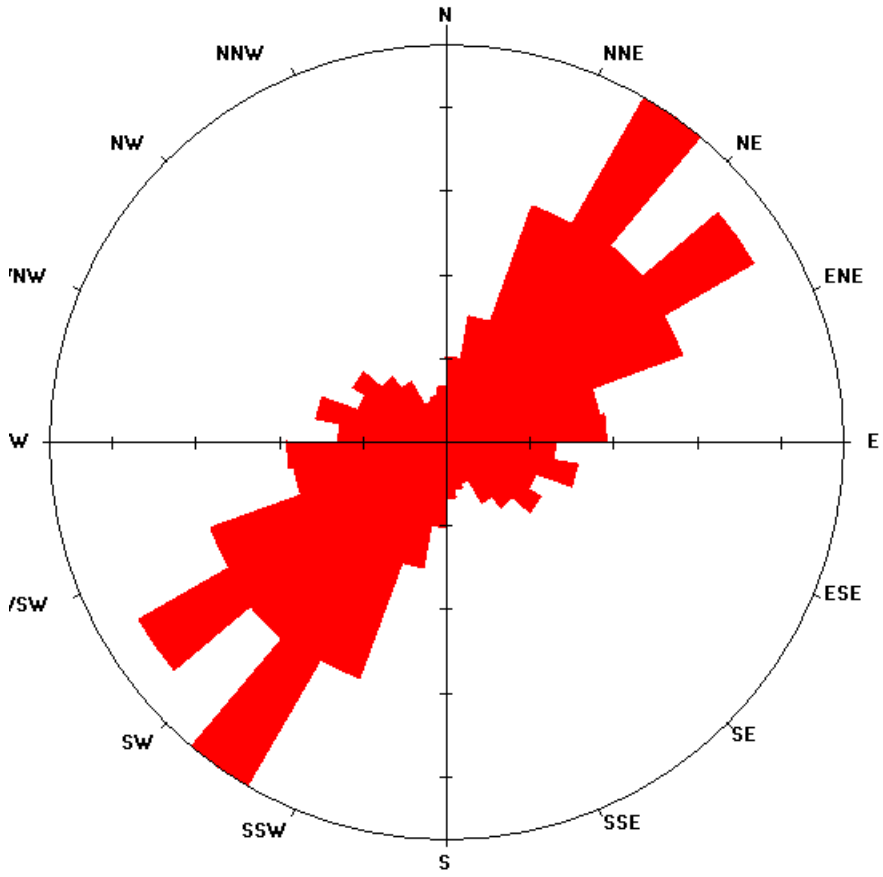

Figure 10*. (a) Rose diagram of lineaments from the Landsat 8 image; (b) Rose diagram of lineaments from the Radarsat image; (c) Rose diagram of lineaments from the Aeromagnetic image*

4.2 Analysis of structural field data

4.2.1 Sedimentary structures

On the field, the original bedding or stratification (S0) is underlined by alternating beds with different sizes of minerals or grading of rock elements. In short, these various syn - sedimentary structures demonstrate the instability tectonic of the basin. This bedding is sometimes quite well preserved in the metasediments (Figure 11, 12). This bedding strikes N020 and dips steeply 76° towards the SE then secondarily towards the NW (Figure 13).

4.2.2 Tectonic structures

The Birimian rocks in the study area are affected by various types of tectonic structures. These structures were identified and characterized in the field through trenching campaigns and core drilling. They have been grouped according to their nature and their geometric and chronological relationships, into Eburnean deformation structures D1, D2 and D3. The quartz veins associated with these deformations are respectively of three types V1, V2 and V3.

4.2.2.1 Deformation D1

To the bedding (S0) often transposes a poorly preserved S1 shearing foliation in metasediments such as sandstones and argillites. It often appears in competent lithologies, as sinistral shear at the contact between Ferkessedougou granite and metasediments (Figure 14). The origin of the S1 shearing foliation is discussed. Could it be linked to peribatholitic deformations (Max et al,. 1996). S1 shearing foliation strikes N003 and dips steeply 83° towards the E (Figure 15). V1 quartz veins are well preserved in the S0 bedding. These V1 veins are laminated bedding veins and strikes N016 and dips gently 58° towards the SE. (Figure 16).

4.2.2.2 Deformation D2

The S2 shearing foliation is well marked in the metasediment units. It is caused by the intrusion of tonalite into the metasediment basement complex (Figure 17). S2 shearing foliation strikes N022 and dips steeply 76 towards the SE then secondarily towards the NW (Figure 18). The types of V2 veins associated with the D2 deformation are of two sets V2a and V2b. The V2a quartz veins are en echelon veins and display a consistent trend of N020 to N040 and the V2b quartz veins strikes between N070 to N090. V2b quartz veins are isolated type veins and sometimes appear as stockworks. The dip of these two sets of veins is 44° towards the NW then secondarily towards SE (Figure 19).

Figure 11. (a) S0 Bedding in argillites

Figure 11. (b) S0 Bedding (N030/70 SE) in argillites. (c) S0 Bedding (N034/67 SE) in argillites

Figure 12. (a) S0 Bedding (N170/82 NE) in sandstones; (b) S0 Bedding (N020/70 NE) in sandstones

Figure 12. (C) S0 Bedding (N034/70 SE) in sandstone, in a valley; (d) S0 Bedding (N022/56 SE) in sandstones

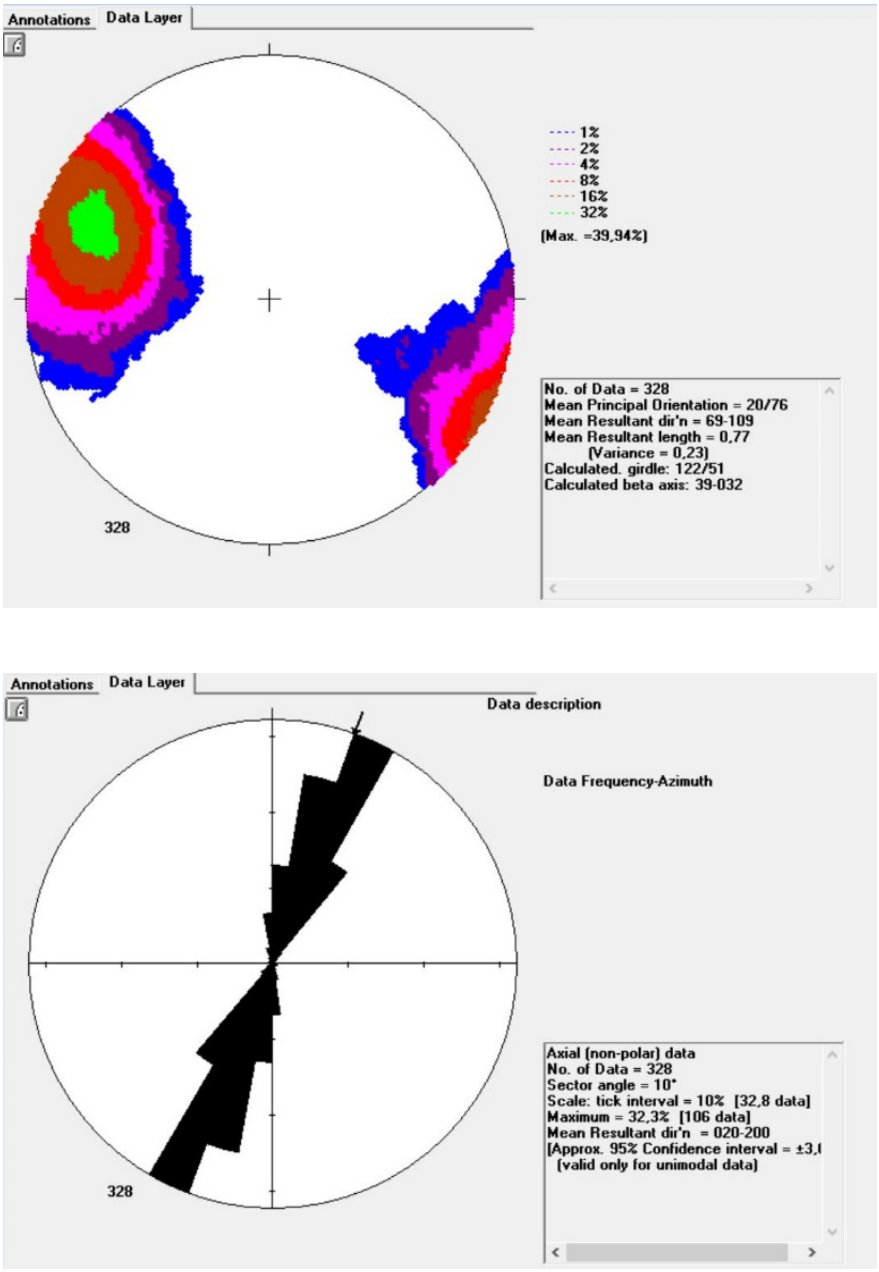

Figure 13 . (a)Rose diagram of the Bedding (S0) N020/ 76 SE with secondarily towards NW; (b) Representation of polars of the Bedding

Figure 14. (a) shearing foliation S1 (N004/58 W) in an intense sinistral shear that marks the contact between batholith (granite) / Argillite; (b) Sinistral shearing S1(N024°/60 SE)

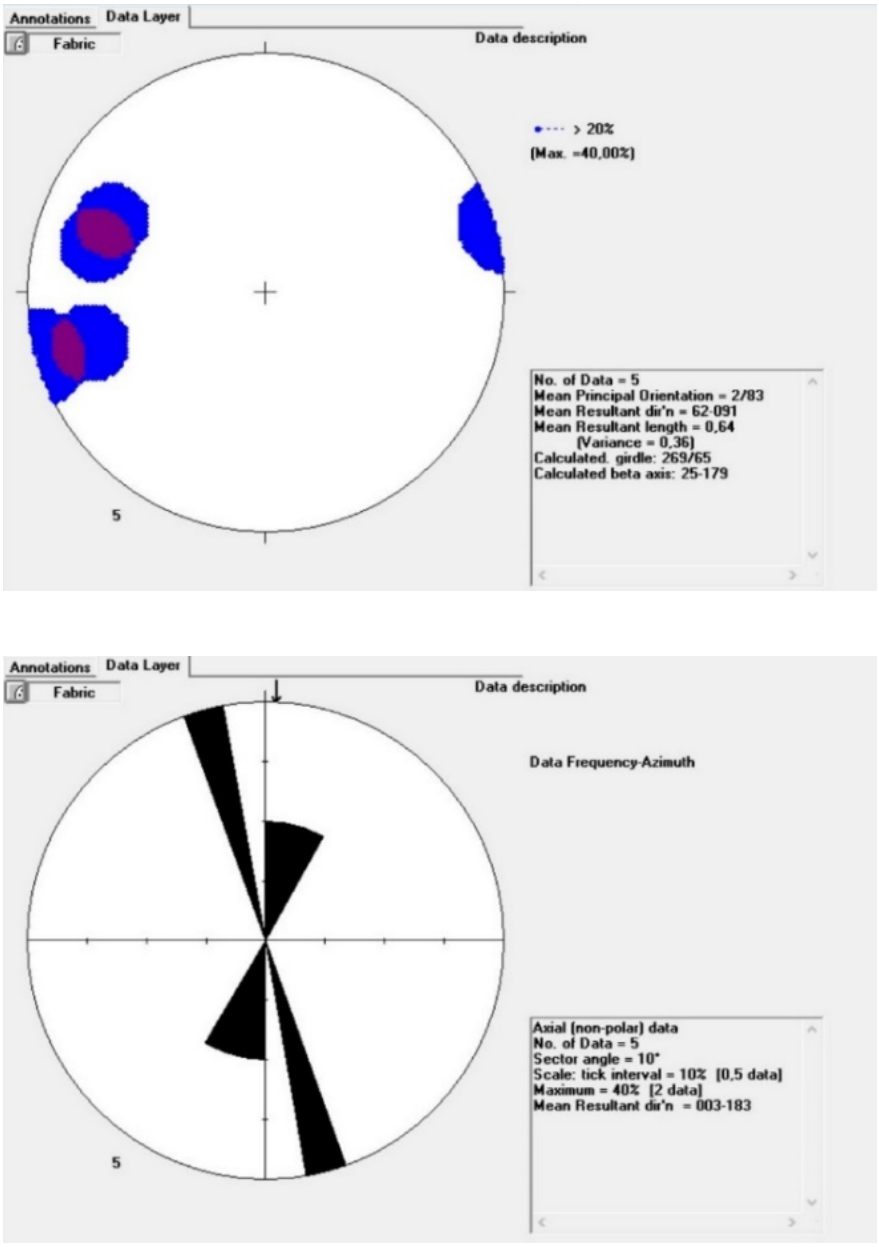

Figure 15 : (a): Rose diagram of shearing foliation (S1) N003/ 83 E; (b): Representation of polars of the shearing foliation(S1)

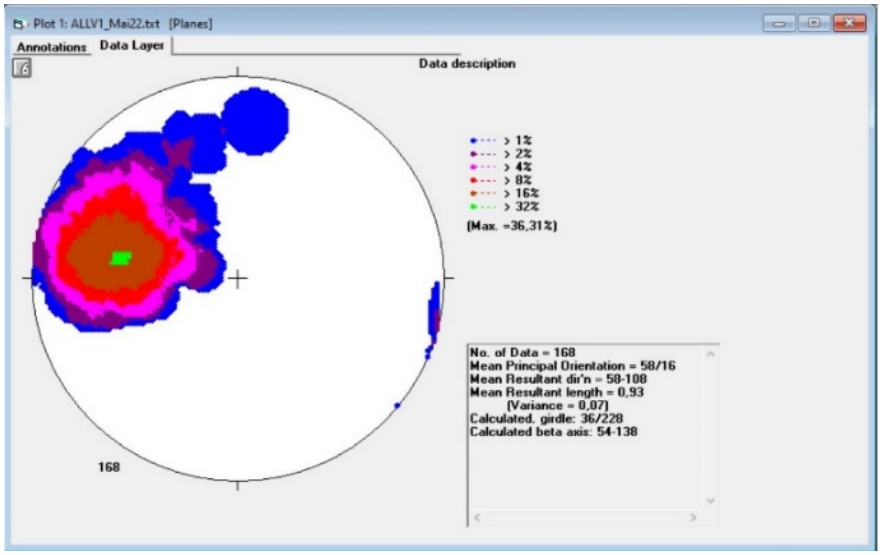

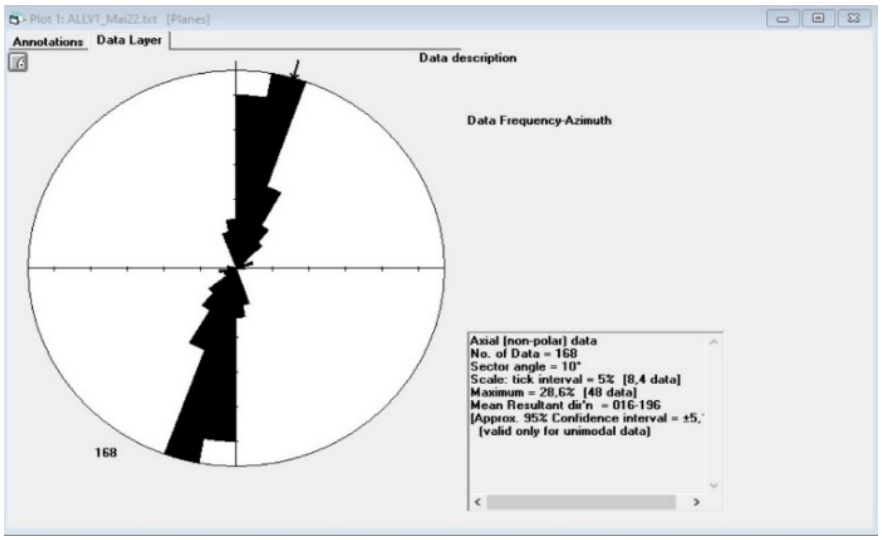

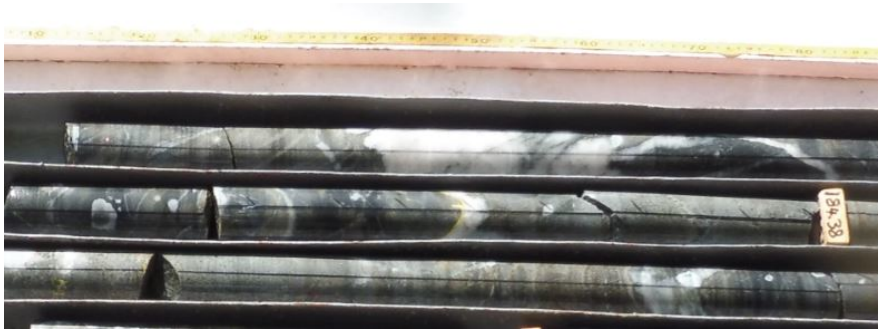

Figure 16. (a): Rose diagram of V1 quartz veins; (b): Representation of polars of quartz veins V1; (c): Quartz vein V1

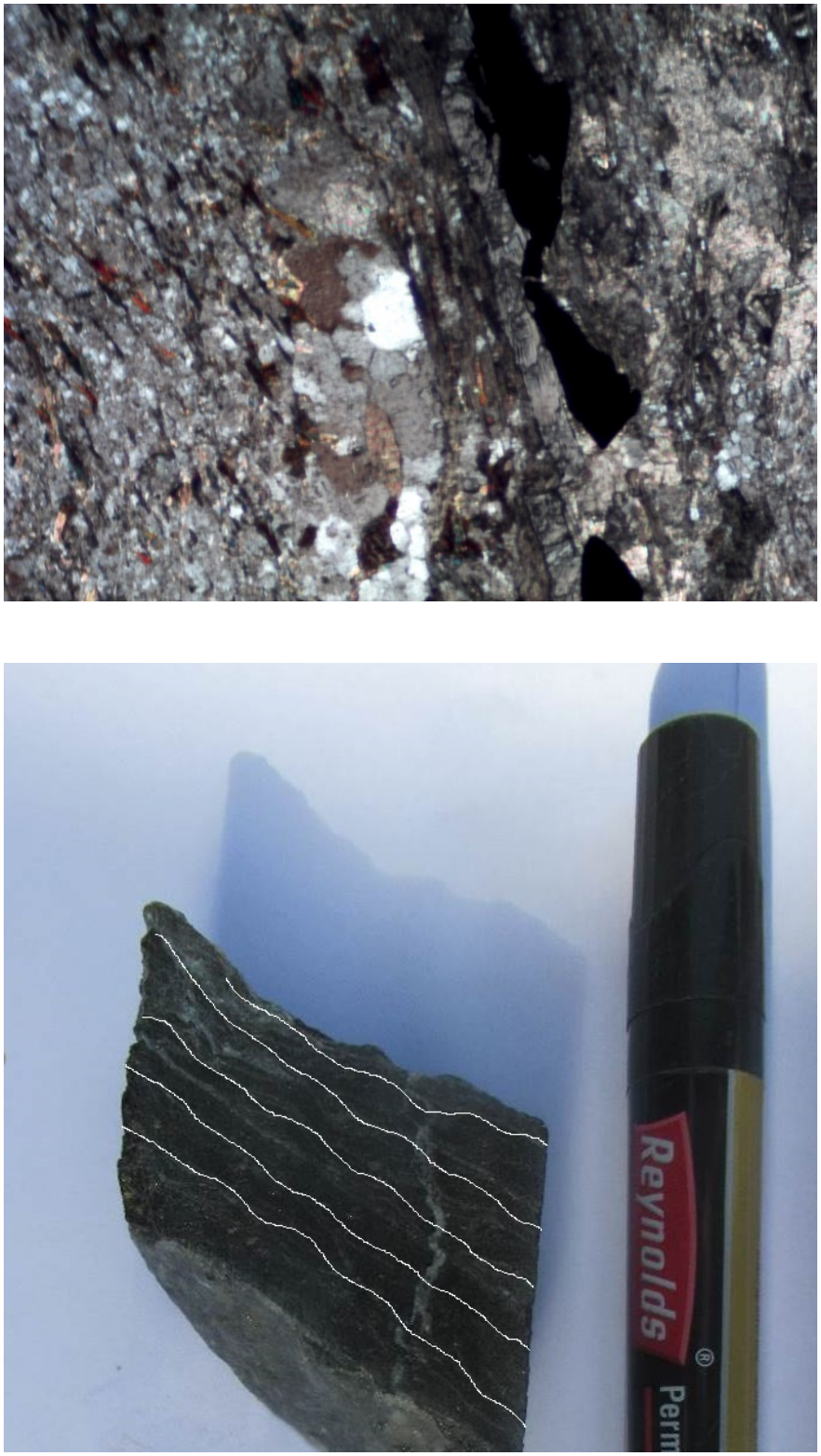

Figure 17. . (a) Shearing foliation S2 (N000/ 54 E) which marks the shearing in the contact between the

Tonalite / sandstone;

(b) Shearing foliation S2 (N000/ 54 E), metallograhic microscope

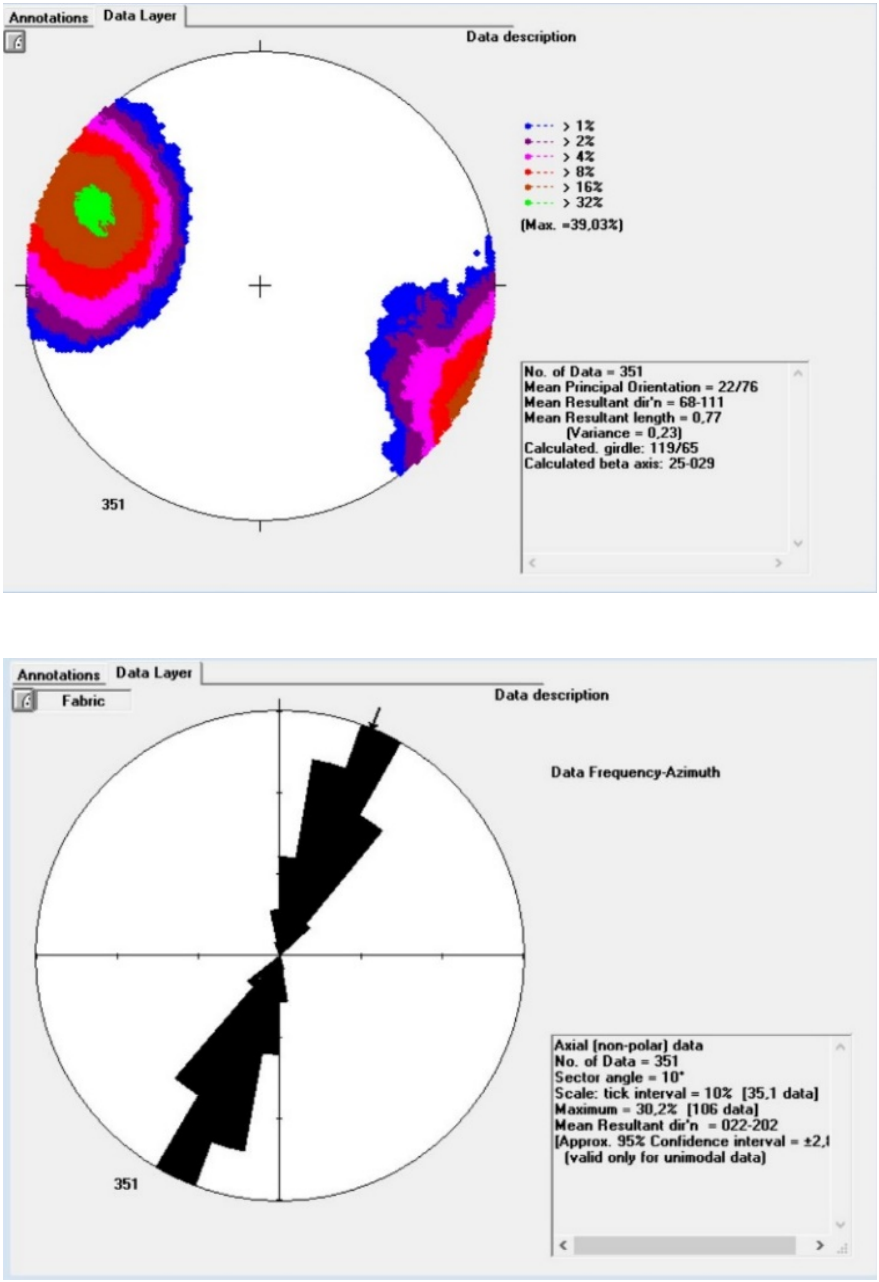

Figure 18. (a):Rose diagram of the Shearing foliation (S2) N022/ 76 SE; (b): Representation of polars of Shearing foliation S2

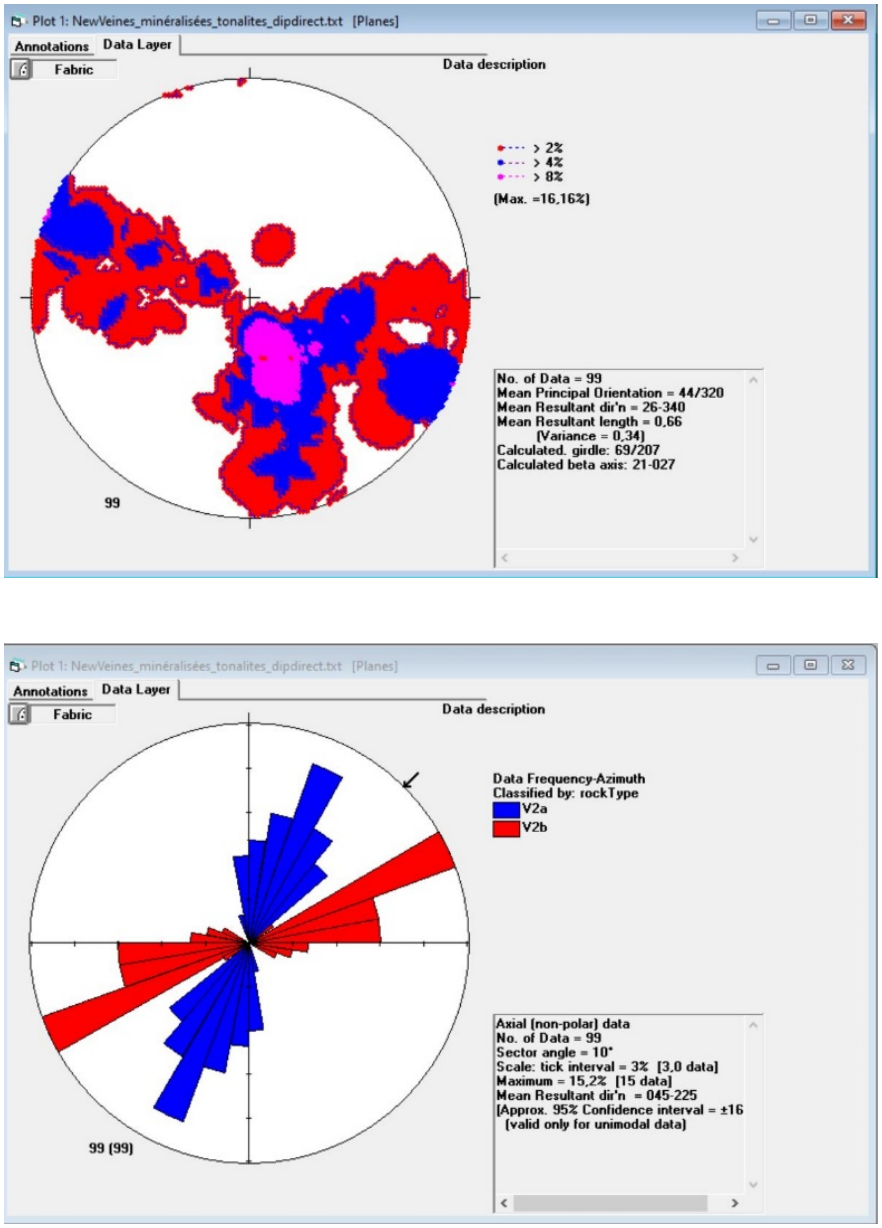

Figure 19. (a): Rose diagram of quartz veins V2a and V2b; (b): Representation of polars of quartz veins V2a and V2b

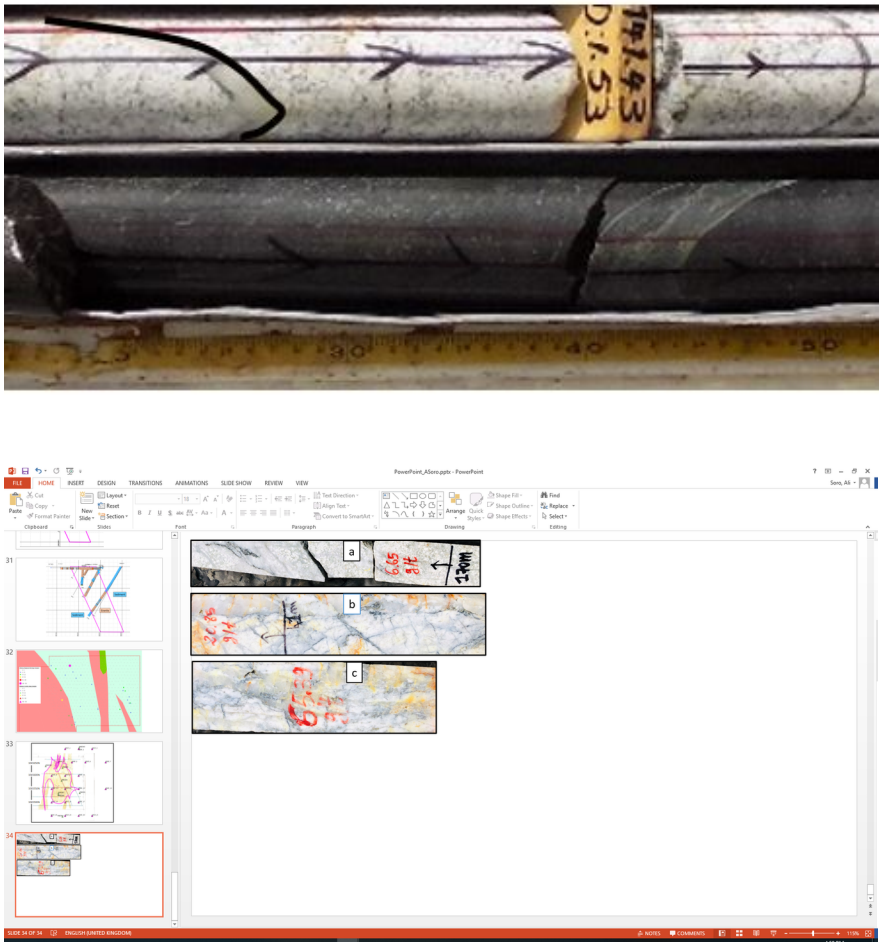

Figure 19. (c): V2a quartz vein; (d): Strongly mineralized quartz vein V2b (65.39 g/t)

4.2.2.3 Deformation D3

The D3 deformation is marked by diorite dykes that cut across the tonalite and metasediments. Diorite dykes were also identified and measured in core drill holes (Figure 20). The dykes strike N010 and dip 66° towards SE (Figure 21). The quartz veins associated with the D3 deformation are V3 veins. They are isolated and trends N044 and dips 85° towards the SE (Figure 22 a, b).

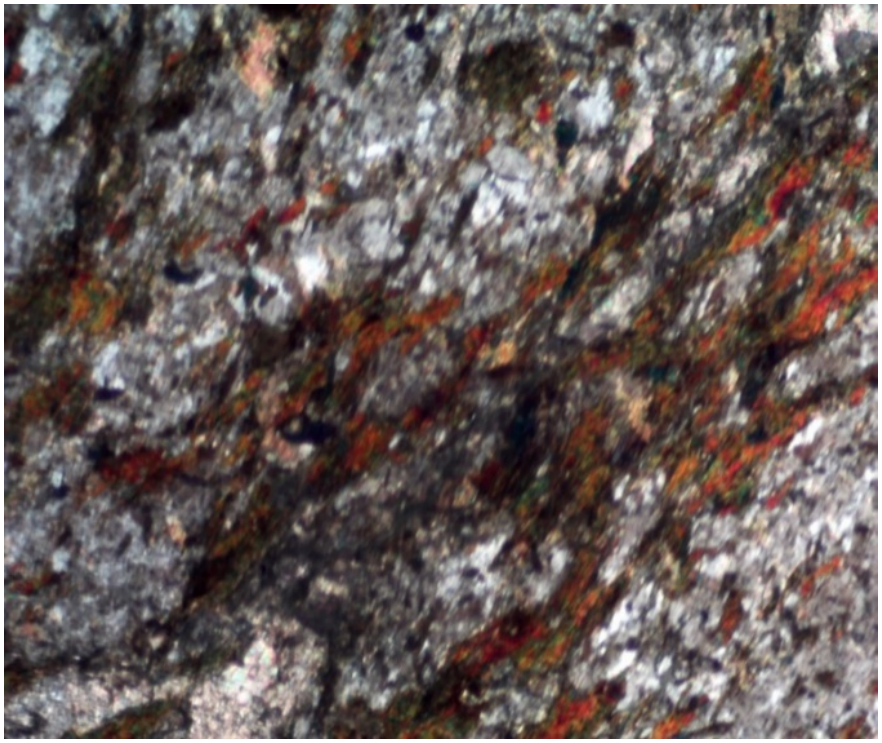

Figure 20: a: Photograh of diorite (TDY013) in drill hole FNDC008@103.3m, showing Shearing foliation S3, Contact Diorite / Sandstone b: Shearing filation S3 in (TDY013) in drill hole FNDC008@103.3m, metallograhic microscope

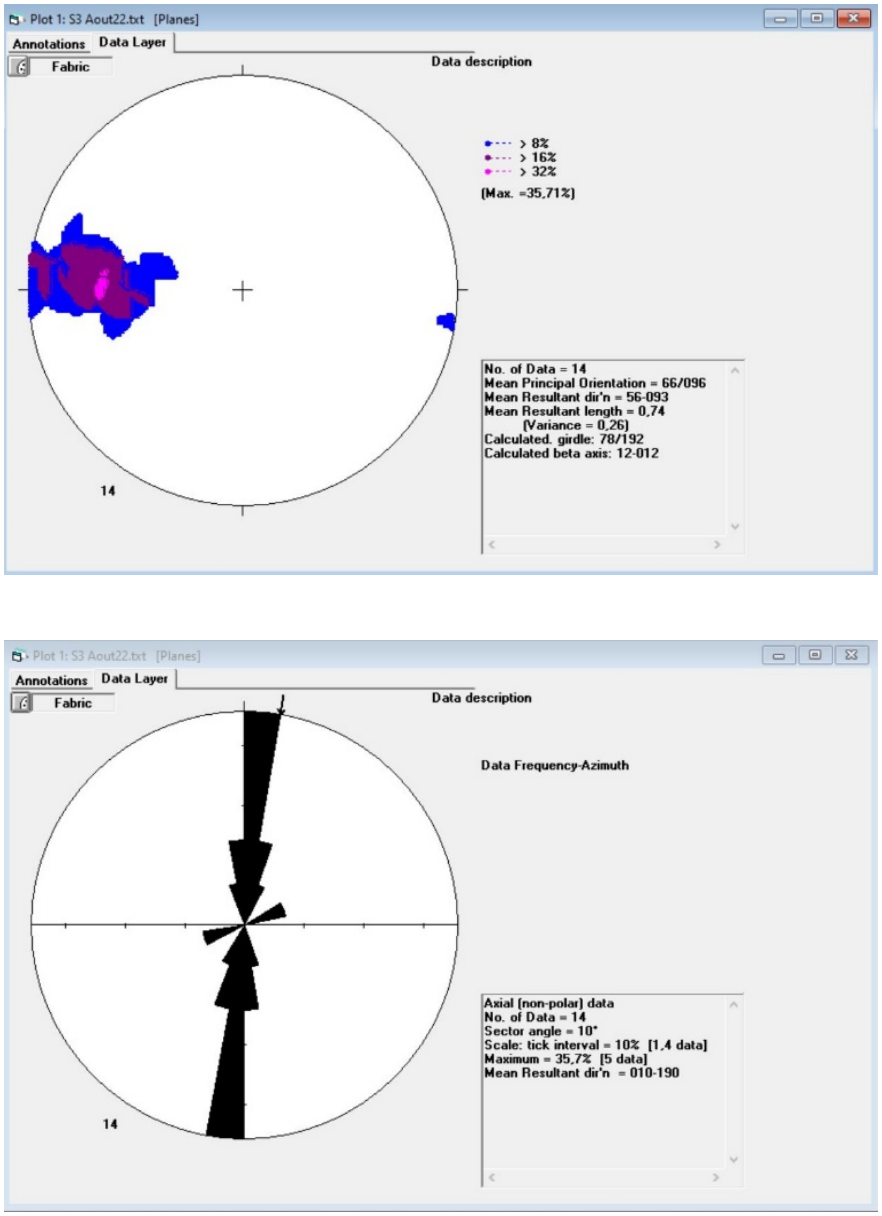

Figure 21. (a) Rose diagram of dyke planes (D3 deformation); (b) Representation of polars dyke

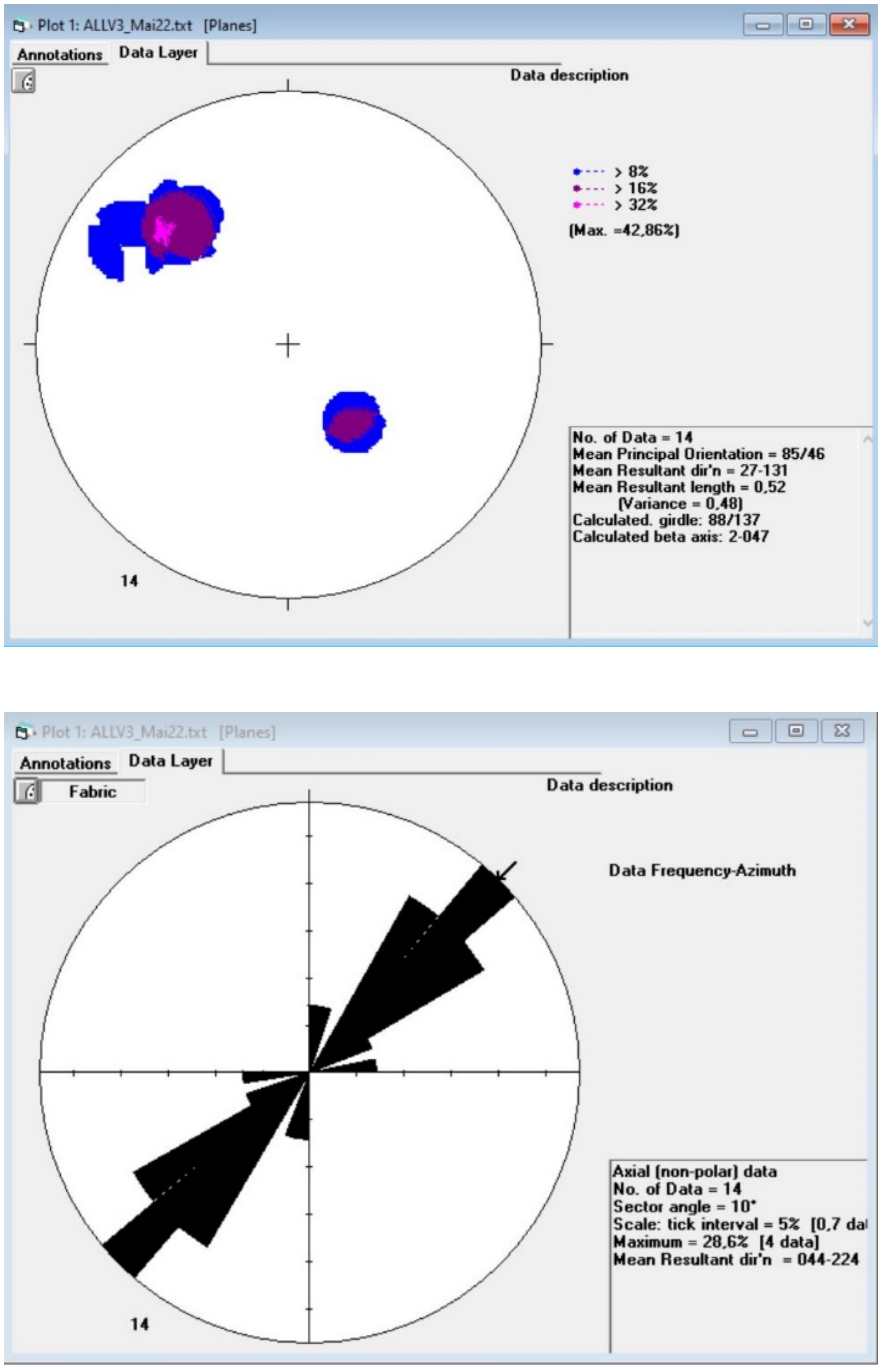

Figure 22. (a): Rose diagram of V3 quartz veins; (b): Representation of polars of V3 quartz vein

5. VALIDATION

The main directions of the lineaments from the Landsat 8 image, Radarsat image and aeromagnetic image are four sets namely the directions N080-N100, N030-050, N000-N020, N120-N135. Relative to the data acquired in the field, we note the D1 deformation in the NS direction with strongly dipping towards east. The S2 shearing foliation of the D2 deformation has a NNE-SSW orientation and a strong dip towards SE

then secondarily towards NW. These directions are respectively in phase with the directions N000-N020 and N030-050 coming from the lineaments. The quartz veins V2b associated with D2 deformation have a N070 -090 orientation and are in phase with the N080-N100 direction of the lineaments.

In conclusion, all lineaments identified from Landat 8, Radarsat and aeromagnetic images have been validated by field data except lineaments N120-N135. On the regional level, the first deformation D1 on the ground corresponds to the Eburnean deformation. The origin of the S1 foliation is discussed. Could it be linked to peribatholitic deformations [20]. On the ground, the S1 foliation transposes onto the S0 bedding. The S1 foliation is difficult to identify and is rarely observed in the field. The D2 regional event corresponds to a NW-SE shortening associated with the first major plutonic event which begins around 2160 Ma and gives numerous granitoid intrusions (Baratoux, and al., 2011), this corresponds to the S2 shearing foliation of the study area. The final phase of deformation corresponds to diorite dykes in the study area and is represented by D3. All these deformations have been represented, and an anticline and a syncline are interpreted in the study area.

The stereonet projections of these deformations shows that the dominant dip of the deformations is towards the SE (Figure 23 and 24) .

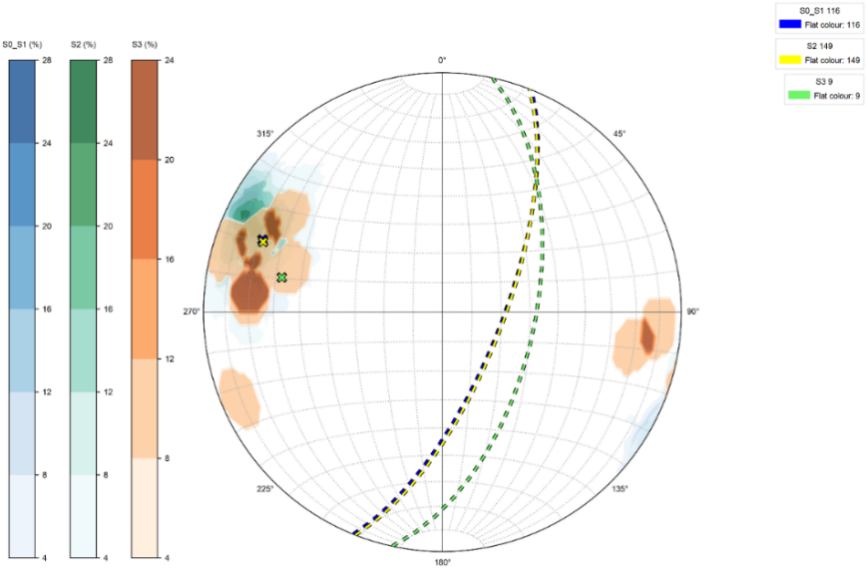

Figure 23. Stereonet projection of deformations (D1, D2, D3) from field dat

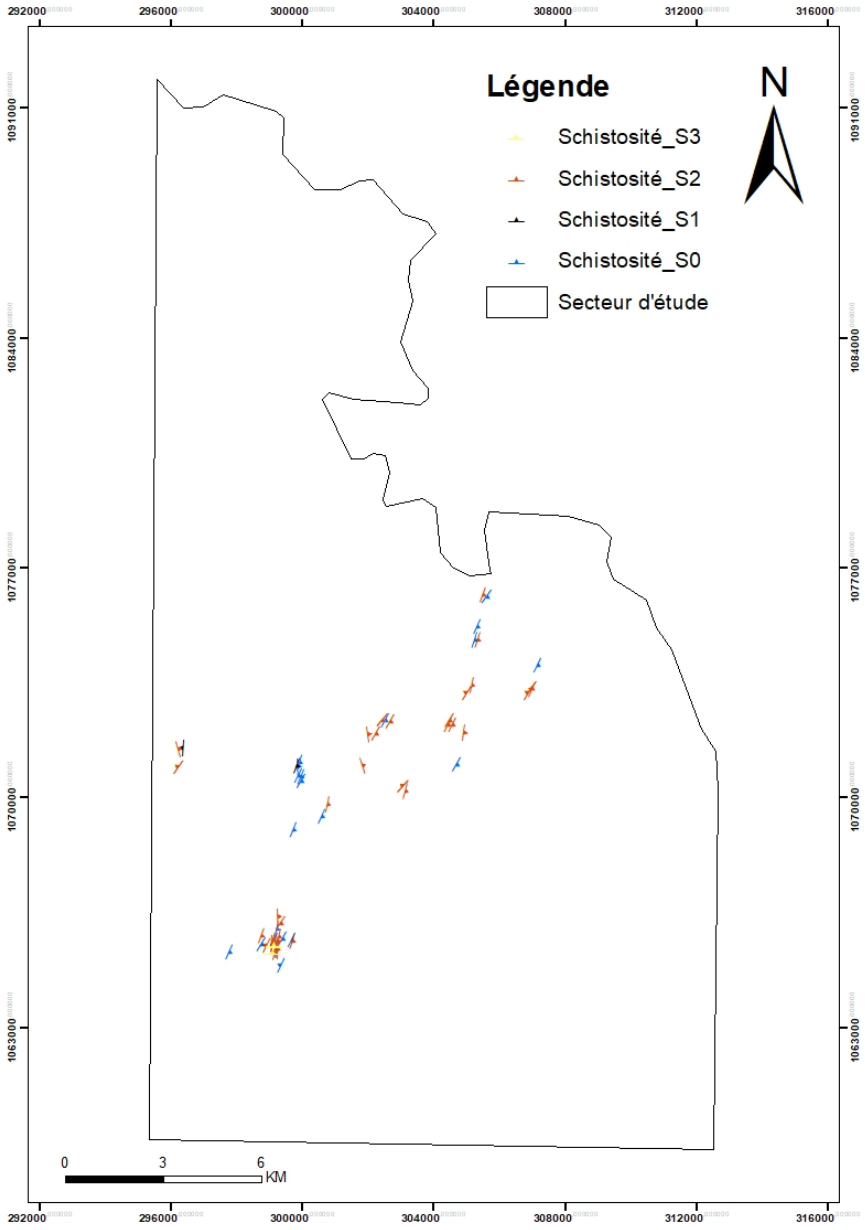

Figure 24. Structural data map of the study area

6.

STRUCTURAL CONTROL OF GOLD MINERALIZATION

Geochemical data have demonstrated that the most mineralized rock is tonalite. A study of the structures that are likely to trap gold in the tonalite has been carried out. According to the statistics made by the Leapfrog software, based on the five core drillings, it is the quartz veins V2b and fractures filled by sulphides then the veins V2a which host the highest gold grades in the tonalite, as indicated by the rose diagram. V2b mineralized strikes between N070 to N090 while V2a mineralized veins strikes N020 to N035. The average dip of all veins is 44° towards NW (Figure 25, 26 and 27). We were able to represent the different mineralized

veins in the tonalite (Figure 28). This confirms that, it is the V2b quartz veins and then the V2a veins that carry the highest grades.

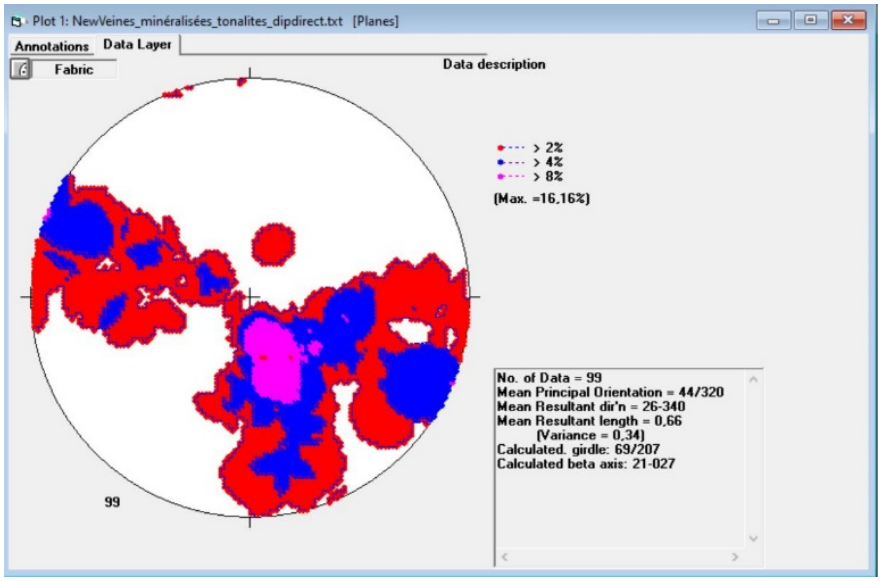

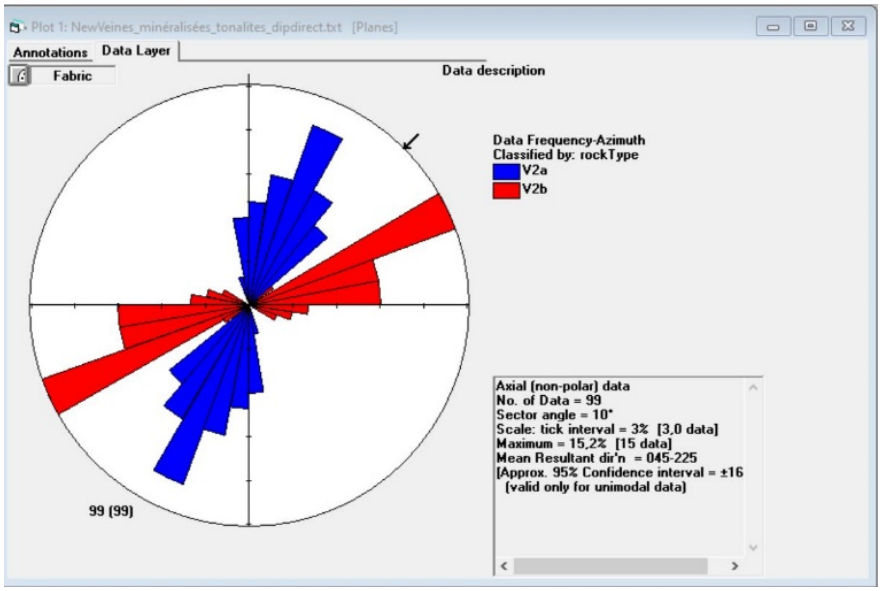

Figure 25. (a) : Rose diagram of all the quartz veins of the tonalite ; (b): Projections of polars of the quartz veins of the tonalite

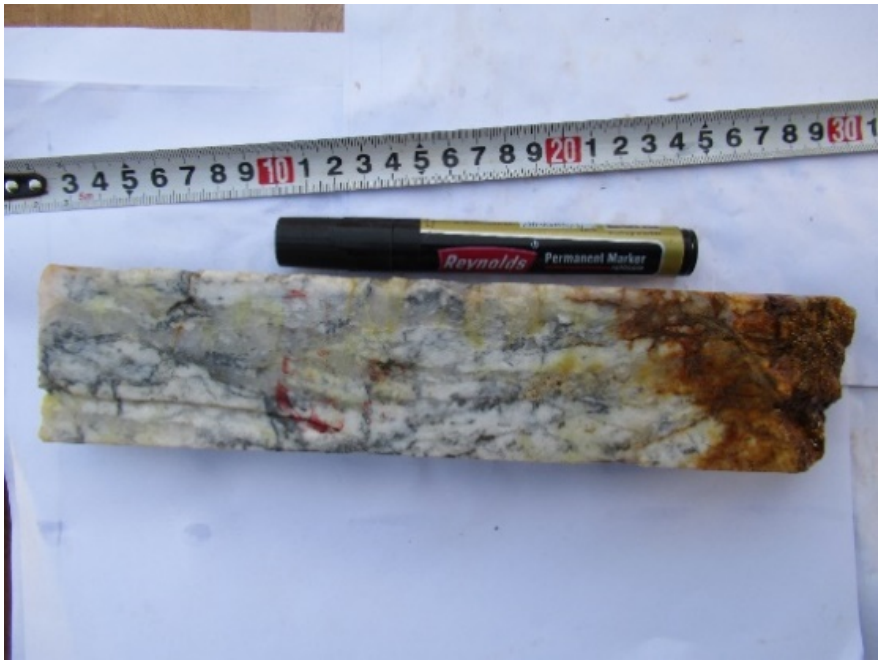

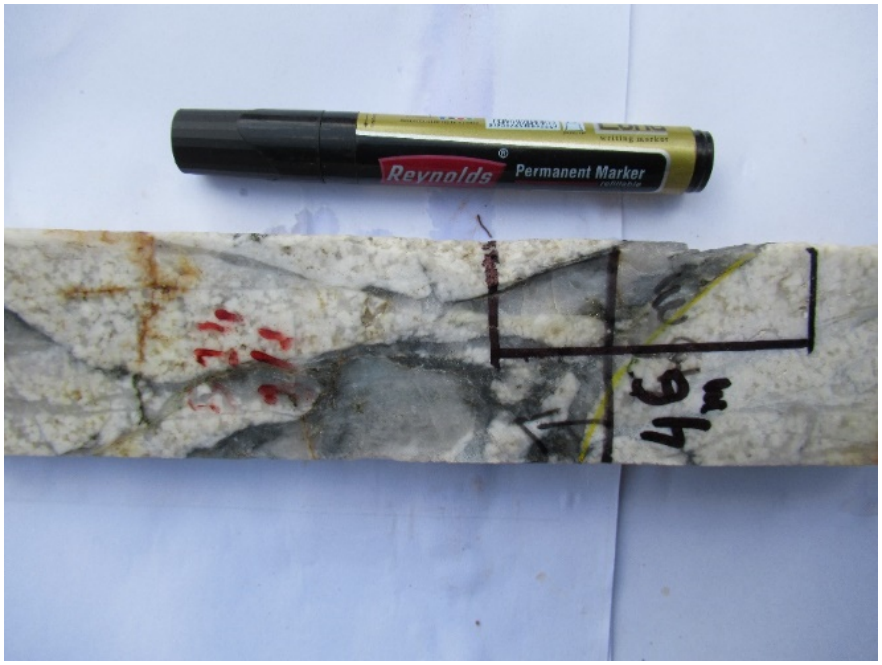

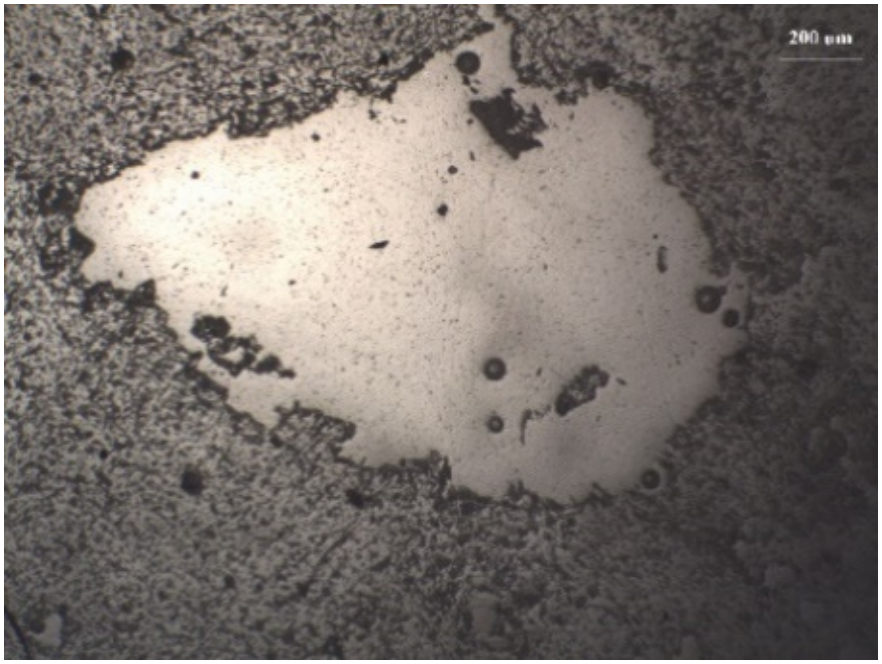

Figure 26. a: Smoky quartz vein (V2a) in tonalite with 26.82 g/t in core drilling hole FNDC012 (PDY005); b: Sulphide hosted in the Smokey Quartz Vein (V2a), metallographic microscope; c: quartz veinlet stockwork (V2b) in tonalite with 65 g/t in core drilling hole FNDC012@40.80m

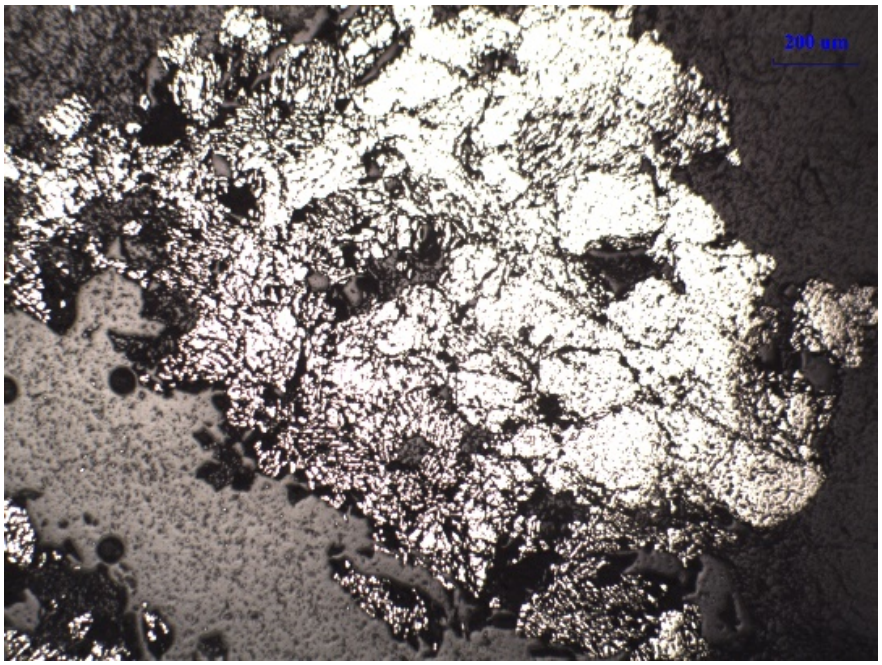

Figure 27 . a: Fracture filled by sulphides in core drilling hole FNDC 008 (PDY 001); b: Sulfide in the fracture, metallographic microscope

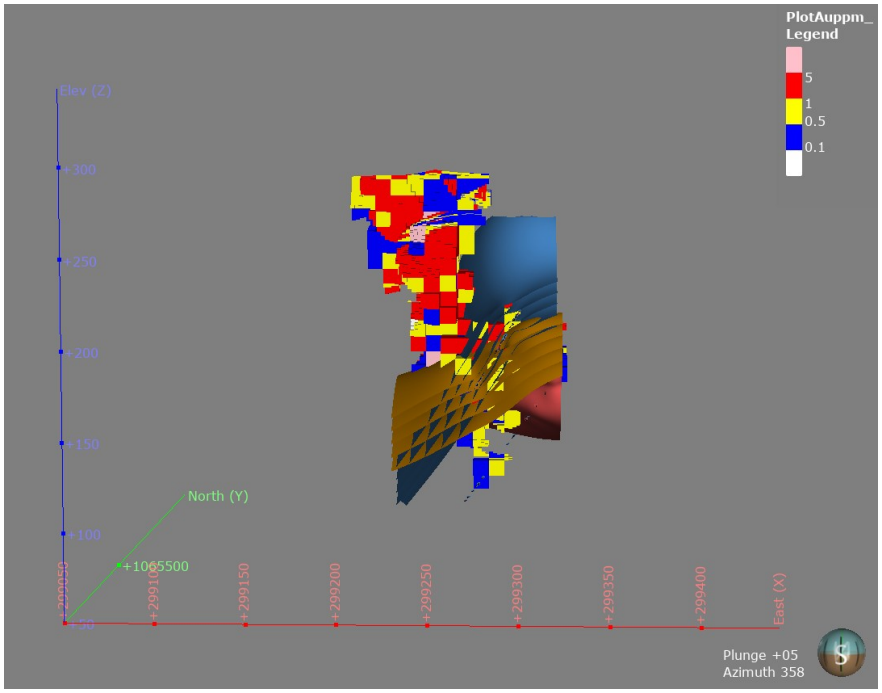

Figure 28. Representation of all quartz veins in tonalite envelope with grades

7. LITHOSTRATIGRAPHY OF THE STUDY AREA

In order to better understand the settng of gold mineralization, meticulous work has enabled the mapping of the Ouarigué prospect to be carried out.

The geology of this prospect is composed from west to east of argillite, tonalite, and sandstone. This tonalite is a small intrusion in the center, and we have the diorite dykes to the east. Then, a more precise block diagram was produced from the trench data and the drilling holes. Structural measurements were taken in order to characterize the mineralized structures. It follows a correlation of the structures coming from the trenches with those of the core drillings hole. This work made it possible to produce this block diagram which presents the different lithologies, the deformations D1, D2 and D3 (Figure 27) .

The lithostratigraphy of the study area is as follows: The setting of the metasedimentary basin on the basement is followed by bedding. Then, the D1 deformation appears and followed by regional metamorphism. Due to the position of the Ferkéssedougou batholith three kilometers west of the prospect, the D1 deformation is insignificant in the study area. Then, there is a tonalite intrusion which introduces the D2 deformation followed by the hydrothermal supply which leads mineralization. Finally, several diorite dykes (D3) intersects this lithological setting and causes another gold mineralization.

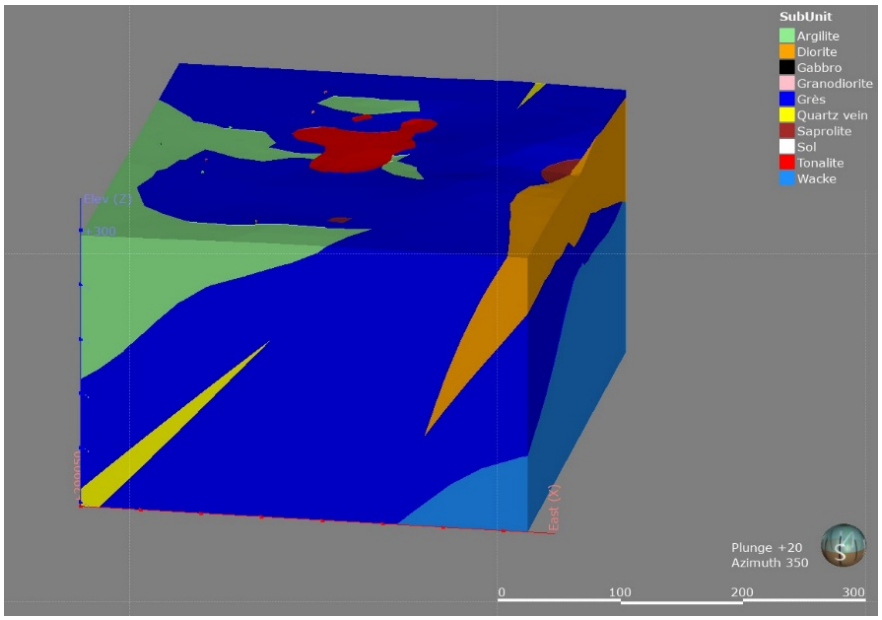

Figure 27. Block diagram of part of the study area

8. TYPE OF MINERALIZATION AND DISCUSSIONS

The study area has similarities with deposits in West Africa. According to Marwitz and al, 2016, there are three IRGS -type deposits in West Africa namely: the Morilla deposit in Mali , the Massawa deposit in Senegal and the Bonikro deposit in Ivory Coast. The Massawa orogenic deposit in Senegal arose from fluids that have a more magmatic origin according to Treloar et al, 2014. Indeed, the Morila mine has been qualified as an IRGS-type deposit by McFarlane et al., 2011. It is a deposit located in the south-east of Mali and hosted in greywackes and volcaniclastics . The mineralized structure is a NNE-SSW trending fold. Several intrusions of leucogranite , quartz diorite and finally muscovite-biotite granites have been identified on this deposit. (MacFarlane and al., 2011). Bonikro deposit was described by Ouattara et al, (2015) as being of the IRGS type in which the gold has a paragenesis Au + Mo+ S + W+ (Bi + Pb +Ag) in

the granodiorite. The Bonikro mine located in the center of Côte d'Ivoire represents an IRGS-type deposit according to the work of Ouattara et al. 2015 (Ouattara and al., 2015). The mineralized rocks of this deposit consist of granodiorite with aplo-pegmatitic dykes with NS-oriented mineralized structures.

However, in the absence of mineralization dating data, the more general classification of Lang and Beker , 2001, was retained. There are three main types of mineralization related to hydrothermal alteration depending on the source of the hydrothermal fluid. Those are:

1) Mineralization linked to extrusive magmatism and volcanism, therefore to hydrothermal cells of seawater and meteoric water leading to the formation of auriferous volcanogenic massive sulphides and epithermal deposits;

2) Mineralization linked to crystallization and the liberation of magmatic fluids (porphyry, Intrusion - related gold system and skarn)

3) Mineralization related to fluids produced during deformation and metamorphism in deep zones of orogeny.

Our study area is of the second type, because it is linked to the crystallization of tonalite. The signature of gold deposits of the "Intrusion- related gold system –IRGS" type is: Au-Bi ±Te ±As ±Mo ±W (Baker, and al., 2001). This metallic signature is partly compatible with the signature of our study area which is Au-Te ±Bi ±Mo± Pb± Re. The mineralization of our study area is therefore the IRGS type.

Conclusion

The lithostratiaphy of the study area consists of a complex basement of metasediments (argillite sandstone and wacke). Then appear the intrusion of the Ferkéssedougou granite, granodiorite and tonalite. Later, diorite dykes crosscut the metasedimentary and the tonalite. Gold mineralization exhibits two forms. Quartz veins control the highest gold grades hosted in tonalite and in contact with metasediment. This mineralization took place during the second phase of deformation characterized by the S2 shearing foliation NNE orientation with a strong dip generally towards the SE but also towards the NW. Finally, the mineralization is affected by the D3 deformation induced by diorite dykes, responsible for another gold mineralization.

References

Baker,T., Lang, J.R., (2001), Fluid inclusion characteristics of intrusionrelated gold mineralization , Tombstone-Tungsten magmatic belt , Yukon Territory , Canada: Mineralium Deposita , c. 36, p. 563–582.*https://doi.org/10.1007/s001260100189*

Baratoux, L., Metelka, V., Naba, S., Jessell, M., Grégoire, M., Ganne J. (2011). Juvenile Paleoproterozoic crust evolution during the Eburnean orogeny (2.2–2.0 Ga), western Burkina Faso. Precambrian Research, 191 p.*https://doi.org/10.1016/j.precamres.2011.08.010*

Bessoles, B. (1977). Geologie de l'Afrique: le Craton Ouest Africain.*Mem. BRGM,* France, 88*,* 403 p.

Biemi, J., Deslandes S., Gwyn, H., Jourda, J.P. (1991). Influence des lineaments sur la productivite des forages dans le bassin versant de la Haute Marahoue (Cote d'Ivoire): Apport de la teledetection et d'un Systeme d'Information a Reference Spatiale". p. 43-49 in Gagnon, P. (ed). Teledetection et gestion des ressources. Vol VII. Comptes rendus du septieme congres de l'Association Quebecoise de Teledetection, 714 p.

Boher M., Abouchami W., Michard A., Albarede F., Arndt N. T. (1992). Crustal growth in West Africa at 2,1 Ga. Journal of Geophysical Research 97, ndeg B1, 345-369.

Djemai, S., Bendaoud, A., H, Haddum., Ouzegane, K., and Kienast, J. R. (2009). Apport des images Landsat 7 ETM+ pour la cartographie geologique des terrains archeens en zone aride : Exemple du terrane de l'In Ouzzal (Hoggar occidentale, Algerie). IIIemes Journees d'Animation Scientifique du reseau de Teledetection

de l'AUF JAS'09, Sous le theme : ¡¡Imagerie Satellitaire Multisources : Approches Methodologiques et Applications¿¿, Alger, 8-11 novembre 2009.

El Gout, R., Khattach, D., Houari, M.-R. (2009). Etude gravimetrique du flanc nord des Beni Snassen (Maroc nord-oriental): implications structurales et hydrogeologiques. Bull Sci 61–75.

Himyari, S.M., Hoepffner, C., Benzakour, M., and Hadani D.E. (2002). Etude structurale du haut atlas oriental Maroc a l'aide de l'analyse lineamentaire des images HRV XS de Spot, Revue Teledetection, vol. 02, ndeg. 4, pp. 243-253.

Jourda, J.P., E.V. Djagoua, K. Kouame, M.B. Saley, C.C. Gronayes, J.-J. Achy, J. Biemi and M. Razack. (2006). Identification et cartographie des unites lithologiques et des accidents structuraux majeurs du departement de korhogo (nord de la cote d'ivoire): Apport de l'imagerie etm+ de landsat. Revue Teledetection, 6(2): 123- 142.

Kouame, K.F., Lasm, T., Saley, M.B., Tonye, E., Bernier, M., and Wade, S. (2009). Extraction lineamentaire par morphologie mathematique sur une image RSO de RadarSat-1 : application au socle Archeen de la Cote d'Ivoire," IIIemes Journees d'Animation Scientifique du reseau de Teledetection de l'AUF JAS'09, Sous le theme : ¡¡Imagerie Satellitaire Multisources : Approches Methodologiques et Applications¿¿, Alger, 8-11 novembre 2009.

Khattach, J.A.D. (2010). Contribution de la gravimetrie a l'etude de la structure des Hauts Plateaux (Maroc oriental). Bull. L'Institut Sci. Rabat 19–30.

Lopez, A., Nezry, E., Touzi R., Laur, H. (1992). Structure detection and statistical adaptive speckle filtering in SAR image. International Journal of Remote Sensing , vol. 14, no. 9, p. 1735-1758. https://doi.org/10.1080/01431169308953999

Masurel, Q. (2015). 4D evolution of the Sadiola-Yatela gold district, Kedougou-Kenieba inlier, West Africa. Ph.D. Thesis, The University of Western Australia, 238 p.

McFarlane, C.R.M., Mavrogenes, J., Lentz, D., King, K., Allibone, A., Holcombe, R. (2011). Geology and Intrusion -related affinity of the Morila Gold Mine, southeast Mali. economic Geology , 106, 727–750. https://doi.org/10.2113/econgeo.106.5.727

Milesi, J.P., Feybesse, J.L., Ledru, P., Dommanget, H.A.S., Ouedraogo, M.F., Marcoux, E., Prost, A., Vinchon, C., Sylvain, J.P., Johan, V., Tegyey, M., Calvez, J.Y & Lagny P. (1989). The gold mineralizations of West Africa, their relations with the lithostructural evolution of the Lower Proterozoic. Chrono. Search _ Min., Fr.497, 98p.1. https://doi.org/10.1016/0301-9268(92)90123-6

Nezry, E., Lopez, A and Touzi, R. (1991). Detection of structural and textural features for SAR images filtering. in proceeding of IGARSS 91, pp. 2169-2172.

Ouattara, G. (1998). Structure du batholite de Ferkessedougou (secteur de Zuenoula, Cote d'Ivoire). Implication sur l'interpretation de la geodynamique du paleoproterozoique de l'Afrique de l'ouest a 2,1 Ga. These de doctorat. Univ. Orleans, 290 p.

Ouattara, Z. (2015). Caracteres lithostratigraphiqie, structural, geochimique et metallogenique du gisement d'or de Bonikro, sillon birimien de Fettekro, centre-sud de la Cote d'Ivoire. Doct. Univ. Felix Houphouet-Boigny, Abidjan, 256 p.

Sonnendrucker, P. (1969). Etude de synthese sur l'or en Cote d'Ivoire, rapport de fin de mission, SODEMI, Abidjan, rapport ndeg222, 127 p.

Ta, M.Y., T. Lasm, J.P. Jourda, F.K. Kouame and M. Razack. (2008). Cartographie des accidents geologiques par imagerie satellitaire landsat-7 etm+ et analyse des reseaux de fractures du socle precambrien de la region de bondoukou (nord-est de la cote d'ivoire). Revue Teledetection 2008 8(2): 119-135.

Tagini, B. (1971). Esquisse structurale de la Cote d'Ivoire. Essai geotechnique regional, These de Doctorat Univ. Fac. Des Sci. Lausannne (Suisse), et, SODEMI, Abidjan, 302 p.

Touzi, R., Lopez, A., Bousquest, P. (1988). A statistical and geometrical edge detector for SAR images. IEEE Transactions on Geoscience , Remote Sensing , vol. 26, no. 6, p. 764-773. doi: 10.1109/36.7708

Treloar, P.J., Lawrence, D.M., Senghor, D., Boyce, A. & Harbidge, P. (2014). The Massawa gold deposit, Eastern Senegal, West Africa: an orogenic gold deposit sourced from magmatically derived fluids ? Geological Society, 27p. https://doi.org/10.1144/SP393.12

Vanie, L.T.A, Khattach, D & Houari, M.R. (2005). Apport des filtrages des anomalies gravimetriques a l'etude des structures profondes du Maroc oriental. Bull. L'Institut Sci. Rabat Sect. Sci. Terre 2005 Ndeg27 29-4 12.

Vanie, L.T.A., Khattach, D., Houari, M.-R., Chourak, M., Corchete, V. (2006). Apport des filtrages des anomalies gravimetriques dans la determination des accidents tectoniques majeurs de l'Anti-Atlas (Maroc), in: Actes Du 3eme Colloque Maghrebin de Geophysique Appliquee. pp. 23–30.

Vidal, M., Delor, C., Pouclet, A., Simeon, Y. & Alric, G. (1996). Evolution geodynamique de l'Afrique de l'Ouest entre 2.2 Ga et 2 Ga: le style "archeen" des ceintures vertes et des ensembles sedimentaires birimiens du nord-est de la Cote d'Ivoire. *Bull. Soc. geol, Fr.,*167, *3:* 307-319.

WAXI, 2018. Geological map of the West African craton

Yao, B.D. (1998) Lithostratigraphie et petrologie des formations birimiennes de Toumodi-Fettekro (Cote-d'Ivoire): implication pour l'evolution pour l'evolution crustale du Paleoproteroique du craton Ouest-Africain. These doc., Univ. Orleans, 191 p.

Yace, I. (2002). Initiation a la geologie. L'exemple de la Cote d'Ivoire et de l'Afrique de l'Ouest. Ed. CEDA, 183 p.

Yesou, H., Pion, J.C., Besnus, Y., and Saint-Jean R. (1993). Amelioration des donnees SPOT pour la cartographie structurale en milieu tropical. Exemple de la region des chapeaux de fer de Pagala Togo), IIIemes Journees Scientifiques du Reseau Teledetection UREF, Toulouse, 13-16 novembre 1990, pp. 143-164.

Tectonics, gold structural control and lithostratigraphy of Ferkessédougou metasedimentary basin, northern Côte d'Ivoire

Zana Yaya Ouattara[1] , Gbélé Ouattara[1]

[1]Department of Civil Engineering, Geosciences and Geographical Sciences, Institut National Polytechnique Félix Houphouët-Boigny, UMRI 68, Yamoussoukro, Côte d'Ivoire.

Correspondence to Email address:

ouattarayayatgl@gmail.com (O. Z. Yaya)

ABSTRACT

The study area is located in the Ferkessédougou belt in northern Côte d'Ivoire, precisely 30 km east of the city of Ferkessédougou. The aim of this study is to understand the tectonic which control gold mineralization. A combination of remote analysis and field mapping work, trenching, reverse circulation drilling hole, core drilling hole was carried out and finally laboratory work (microscopy). Different processing such as ACP, adaptive filters have been applied to Landsat 8 and Radarsat satellite images, in order to enhance information for better lineament extraction. Also, different complementary techniques (horizontal gradient, Euler deconvolution) were applied to the areomagnetic map in order to highlight the different lineaments. Four sets of lineaments have been producted by these images: N080-N100, N030-050, N000-N020, N120-N135.The validation of these different linear structures was made by field data. Thus, in the field, the metasediments show a strong S1 shearing stirikes NNE, with and dips towards the South-East, compatible with a D1 shortening episode. The emplacement of leucogranitic batholith and tonalite induces deformation (D2) which is shearing foliation S2. Later, diorite dykes induces the S3 shearing foliation. The earliest form of gold mineralization is located in quartz veins and fractures filled by sulphide (pyrite). The second form of gold mineralization is disseminated and hosted in the sheared contacts betwween intrusive units with the metasediments. Studies show that quartz veins control the highest gold grades in tonalite unit. The mineralization of our study area is an IRGS type.

Keywords: Gold, mineralization, Pyrite, Ferkessedougou, Ivory Coast, West Africa Craton.

Introduction

The significant West Africa's gold production hosted by Birimian's rocks (Milesi et al., 1989). In addition, gold production in recent years located in the Paleoproterozoic domain is the strongest growth in the world (Masurel, 2015). Seventeen Birimian belt are distributed over two reference alignments, Tehini-Dimbokro in the East and Ferkessedougou - Soubré in the center have been identified in Côte

d'Ivoire (Tagini, 1971; Yace, 2002). Our study area is located thirty (30) km eastern of the town of Ferkessedougou, in northern Côte d'Ivoire and situated in the belt of Ferkessédougou which is subject of exploration and artisanal mining. This belt has been identified as a gold region in the geostructural classification gold-bearing regions of Côte d'Ivoire (Sonnendrucker, 1969). This study will allow us to carry out the chronology of various deformations, as well as the model of gold mineralization in this area.

1. GEOLOGICAL CONTEXT

Ivory Coast is located in the southern part of the West African craton, precisely on the Man Ridge (Bessoles, 1977). It comprises two large unevenly distributed geological units which are, on the one hand, a narrow coastal sedimentary basin bordering the Gulf of Guinea in the south of the country and, on the other hand, a crystalline basement of Precambrian age which covers 97.5% of the national territory. The Pre-Ecambrian basement of Côte d'Ivoire is subdivided into two major domains depending on the age of the formations encountered, which are: (i) the Archean domain formed of crystalline and crystallophyllian rocks and (ii) the Paleoproterozoic domain formed of rocks crystalline and meta - volcano - sedimentary (Figure 1) (Bessoles, 1977). These two domains of unequal areas are separated by the Sassandra fault with sinistral movement oriented North-South. The Paleoproterozoic domain in which our study area is located was structured by the Eburnean megacycle. The formations of this domain in Côte d'Ivoire are volcano-sedimentary belt generally oriented NNE-SSW (Tagini, 1971; Daouda, 1998). On a regional scale, the study area is composed from west to east: of a biotite granite, metasediments namely: sandstones and argillites and finally a granodiorite to the west. The study area is composed from west to east: of a granite, volcanosediments and the sequence: argillites, pelites and shale (Figure 2) (WAXI, 2018). This granite located to the west of the study area is a vast and very extensive pluri-plutonic batholith (more than 500 km in length), it is an assembly of small two-mica plutons relatively similar in shape to laccoliths (Ouattara, 1998).

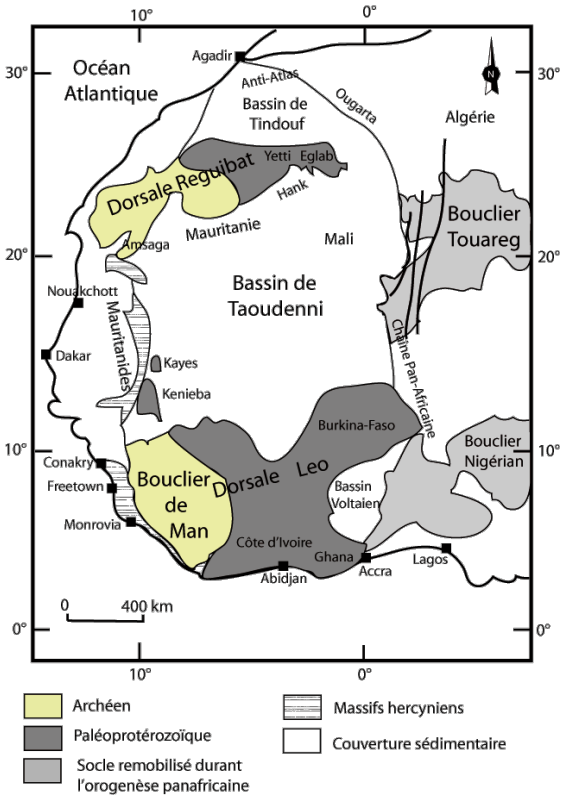
10°
0°
30°
20°
10°
0°
Océan Atlantique
Agadir
Anti-Atlas
Ougarta
Bassin de Tindouf
Algérie
Yetti Eglab
Hank
Dorsale Reguibat
Mauritanie
Amsaga
Mali
Bouclier Touareg
Bassin de Taoudenni
Nouakchott
Mauritanides
Chaîne Pan-Africaine
Dakar
Kayes
Kenieba
Burkina-Faso
Bouclier Nigérian
Conakry
Freetown
Monrovia
Bouclier de Man
Dorsale Leo
Bassin Voltaien
Côte d'Ivoire
Ghana
Accra
Lagos
Abidjan
0 400 km
Archéen
Paléoprotérozoïque
Socle remobilisé durant l'orogenèse panafricaine
Massifs hercyniens
Couverture sédimentaire

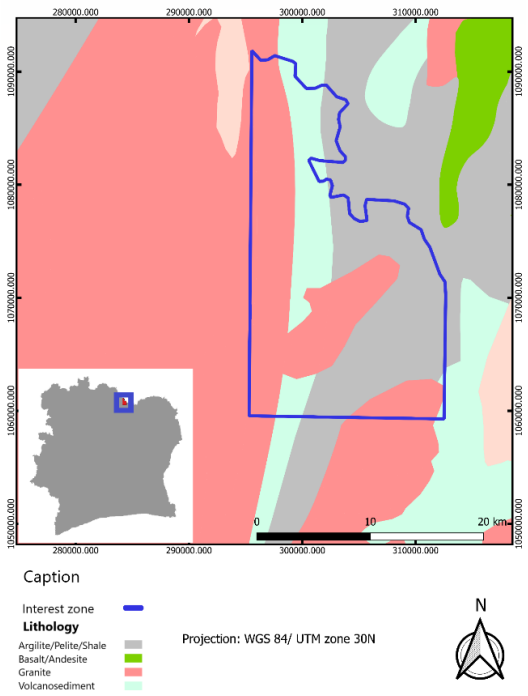

Figure 1: Shematic map of West Africa Craton (Boher et al., 1992)

Figure 2. Presentation of the study area on geological map of WAXI (2018)

2. MATERIAL

The equipment used to carry out this work includes remote analysis data and field data. Remote analysis data includes satellite image Landsat 8 and the radarsat image. In addition to these images, there is the geological map of WAXI 2018. The images were downloaded and processed from softwares. These are Landsat 8 optical image, radarsat image of the study area. Satellite images Landsat 8 were downloaded from the website at http://www.earthexplorer.usgs.gov. According to Landsat image, we used a total of 11 images (bands 1, 2, 3, 4, 5, 6-1, 6, 7, 8, 9, 10 and 11). Aeromagnetic image has been treated also.The survey was carried out by Kenting Earth Sciences Ltd, during the years 1974 and 1975 as part of a cooperation program between the Government of Canada and Côte d'Ivoire.The softwares used for image processing are Envi, Arc Gis, Google Earth Pro and Qgis, Geosoft. Structural data was processed with Global Mapper, Georient and Leapfrog softwares.

3. METHODS

Relative to the landsat 8 image, the band 8 has been choosen. The band 8 is the panchromatic band with a resolution of 15 meters on the ground. After atmospheric and radiometric corrections applied to band 8, Principal Composi-

tion Analysis (PCA) and various processing filters were applied to enhance the perception of linear structures. PCA is an effective technique which allows to accentuate multi-spectral images for fine geological interpretations (Biémi et al., 1991) because it allows to reduce the information contained in several bands, sometimes highly correlated (redundancy of spectral information) in a number more restricted of components. Component 1 (band 1 of PCA) was retained. Therefore, we have chosen to apply the filter to this first principal component. Filters have also been applied to the radarsat image. Filtering consists in changing the value of a pixel according to those of its neighbors (Touzi et al., 1988, Nezry, et al., 1991; Lopez, et al., 1992; Yésou, et al., 1993). We applied the four Sobel filters, the PREWITT filter and the YESOU filter to the two images. These directional filters whose application matrices make it possible to bring out or mask specific characteristics of an image based on their frequency related to texture (Himyari, et al., 2002; Jourda, et al., 2006; Ta, et al,. 2008; Djemai, et al., 2009; Guergour, et al., 2009; Kouamé, et al., 2009). Then, the flowchart of the processing carried out on the images is presented in figure 3. The lineament maps resulting from these images were obtained. Finally, we validated the Landsat image and the radarsat image using the field data and pre-existing maps. After extracting the study area from the raw aeromagnetic map, the processing consists of applying specific filters. We successively applied the horizontal and vertical derivatives and the magnitude of the horizontal gradient. The calculation of the Euler deconvolution, by applying the structural index "1", made it possible to highlight faults at depth and to follow their connection with the faults affecting the cover in accordance with the work of (Vanié and al., 2005, Vanié et and., 2006, El Gout et al., 2009, Khattach, 2010). The results of the various treatments are presented as lineament maps and rose diagram. (Vanié et al., 2006).

Figure 3.a Landsat8 Image processing flowchart; **b** Radarsat Image processing flowchart; **c** AeromagImage processing flowchart

During the differents geological mapping campaigns, the rare outcrops that appear in contact with the granite Ferkessedougou batholith and the metasediments, along the watercourses and finally along the tracks allowed us to identify several structural elements. Although some outcrops are not directly located on the mineralization, nevertheless they offer several east-west sections through the granite contact (Ferkessedougou batholith) and the metasediments. Also, it will be necessary to add the cartography of 7100m in length of thirty-seven (37) trenches during which nine hundred eighty-seven (987) structures were measured and one thousand nine hundred and sixty (1960) structures from nine (19) core drilling. The planar structures are bedding, shearing foliation, veins or sometimes quartz and carbonates veinlets. All of these data have been classified according to their nature and their chronological relationship, in to deformation structures D1, D2 and D3.

4. RESULTS

4.1 Images data

After image processing, lineament maps from Landsat 8, Radarsat and aeromagnetic images were obtained. The rose diagram were made from these lineament maps. The raw Landsat 8 image as well as the lineament map of the image are presented below (Figure 4 and 5). The radarsat image and its lineament map are presented below (Figure 6 and 7). the Aeromag image and its lineament map are presented below (Figure 8 and 9).

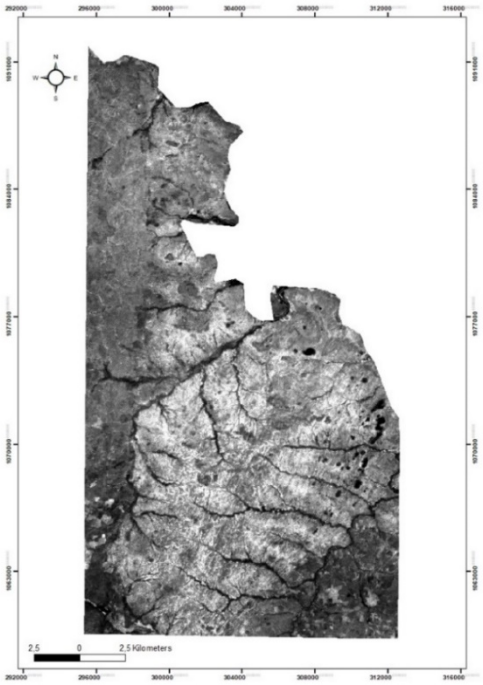

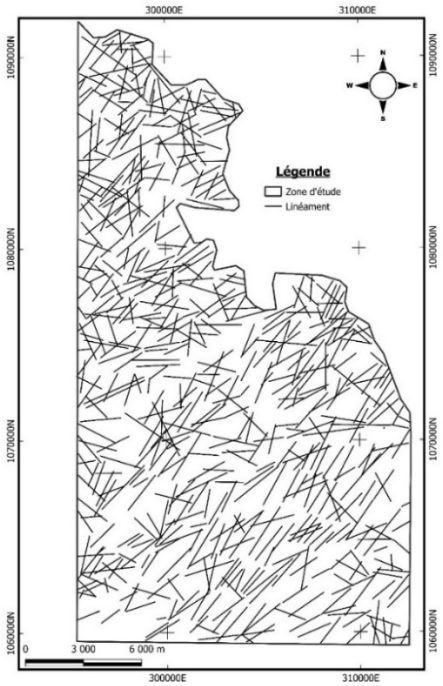

Figure 4. *Raw Landsat 8 image* ***Figure 5.*** *Lineament map from Landsat 8 image*

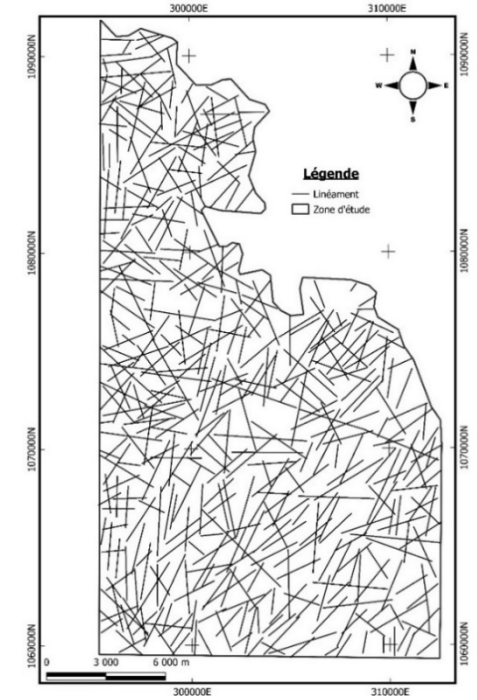

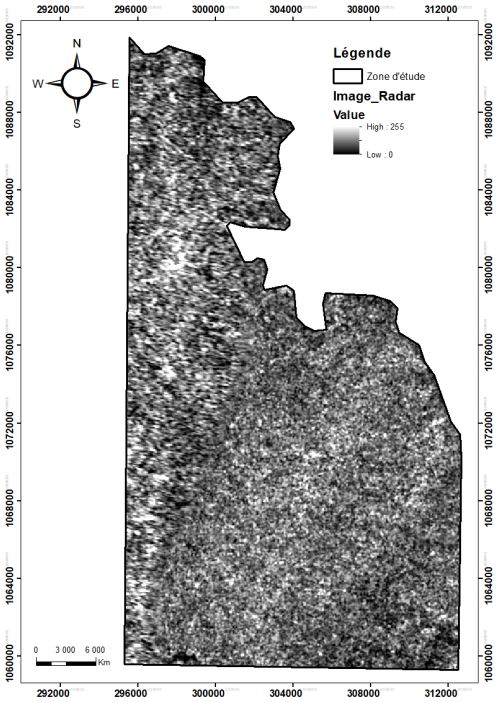

Figure 6. *Raw Radarsat image* ***Figure 7.*** *Lineament map from the radarsat*

image

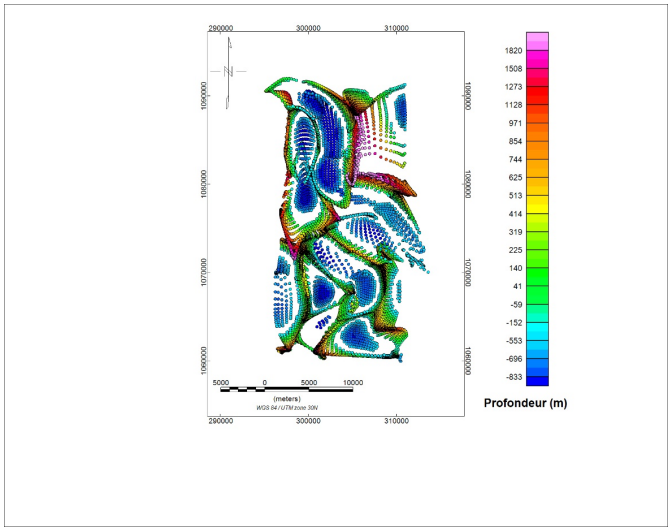

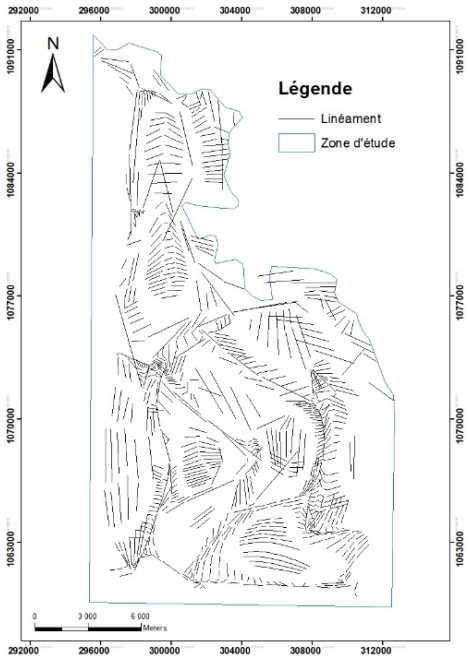

Figure 8. *Euler's solution map* ***Figure 9.*** *Lineament map from aeromagnetic image*

After the analysis of lineament maps from landsat 8 and radarsat, aeromagnetic images, the main directions of lineaments are presented as four sets namely N080-N100, N030-050, N000-N020, N120-N135. We will compare these results

with field data (Figure 10).

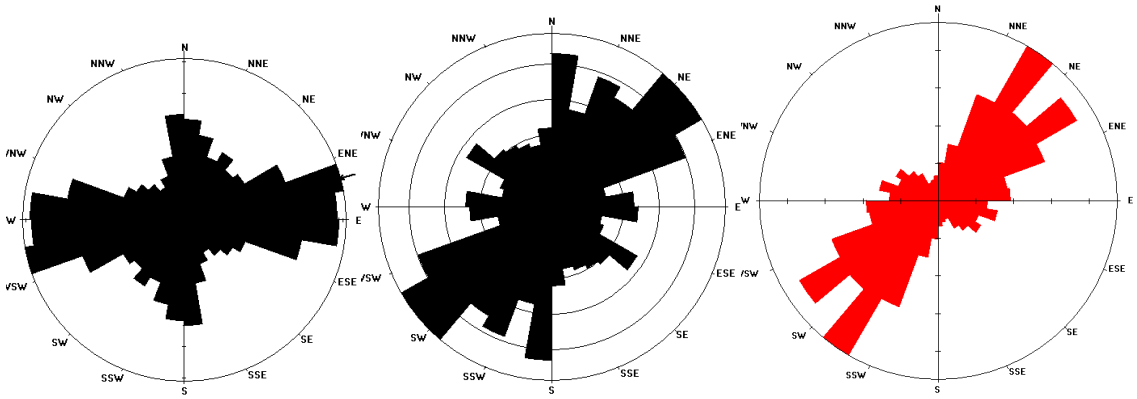

Figure 10*. (a) Rose diagram of lineaments from the Landsat 8 image; (b) Rose diagram of lineaments from the Radarsat image; (c) Rose diagram of lineaments from the Aeromagnetic image*

4.2 Analysis of structural field data

4.2.1 Sedimentary structures

On the field, the original bedding or stratification (S0) is underlined by alternating beds with different sizes of minerals or grading of rock elements. In short, these various syn - sedimentary structures demonstrate the instability tectonic of the basin. This bedding is sometimes quite well preserved in the metasediments (Figure 11, 12). This bedding strikes N020 and dips steeply 76° towards the SE then secondarily towards the NW (Figure 13).

4.2.2 Tectonic structures

The Birimian rocks in the study area are affected by various types of tectonic structures. These structures were identified and characterized in the field through trenching campaigns and core drilling. They have been grouped according to their nature and their geometric and chronological relationships, into Eburnean deformation structures D1, D2 and D3. The quartz veins associated with these deformations are respectively of three types V1, V2 and V3.

4.2.2.1 Deformation D1

To the bedding (S0) often transposes a poorly preserved S1 shearing foliation in metasediments such as sandstones and argillites. It often appears in competent lithologies, as sinistral shear at the contact between Ferkessedougou granite and metasediments (Figure 14). The origin of the S1 shearing foliation is discussed. Could it be linked to peribatholitic deformations (Max et al,. 1996). S1 shearing foliation strikes N003 and dips steeply 83° towards the E (Figure 15). V1

quartz veins are well preserved in the S0 bedding. These V1 veins are laminated bedding veins and strikes N016 and dips gently 58° towards the SE. (Figure 16).

4.2.2.2 Deformation D2

The S2 shearing foliation is well marked in the metasediment units. It is caused by the intrusion of tonalite into the metasediment basement complex (Figure 17). S2 shearing foliation strikes N022 and dips steeply 76 towards the SE then secondarily towards the NW (Figure 18). The types of V2 veins associated with the D2 deformation are of two sets V2a and V2b. The V2a quartz veins are en echelon veins and display a consistent trend of N020 to N040 and the V2b quartz veins strikes between N070 to N090. V2b quartz veins are isolated type veins and sometimes appear as stockworks. The dip of these two sets of veins is 44° towards the NW then secondarily towards SE (Figure 19).

Figure 11. (a) S0 Bedding in argillites

Figure 11. (b) S0 Bedding (N030/70 SE) in argillites. (c) S0 Bedding (N034/67 SE) in argillites

Figure 12. (a) S0 Bedding (N170/82 NE) in sandstones; (b) S0 Bedding (N020/70 NE) in sandstones

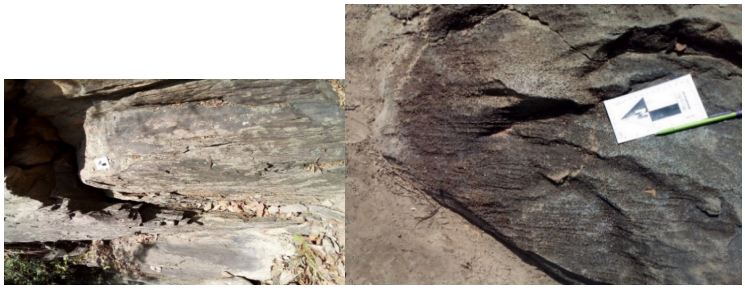

Figure 12. (C) S0 Bedding (N034/70 SE) in sandstone, in a valley; (d) S0 Bedding (N022/56 SE) in sandstones

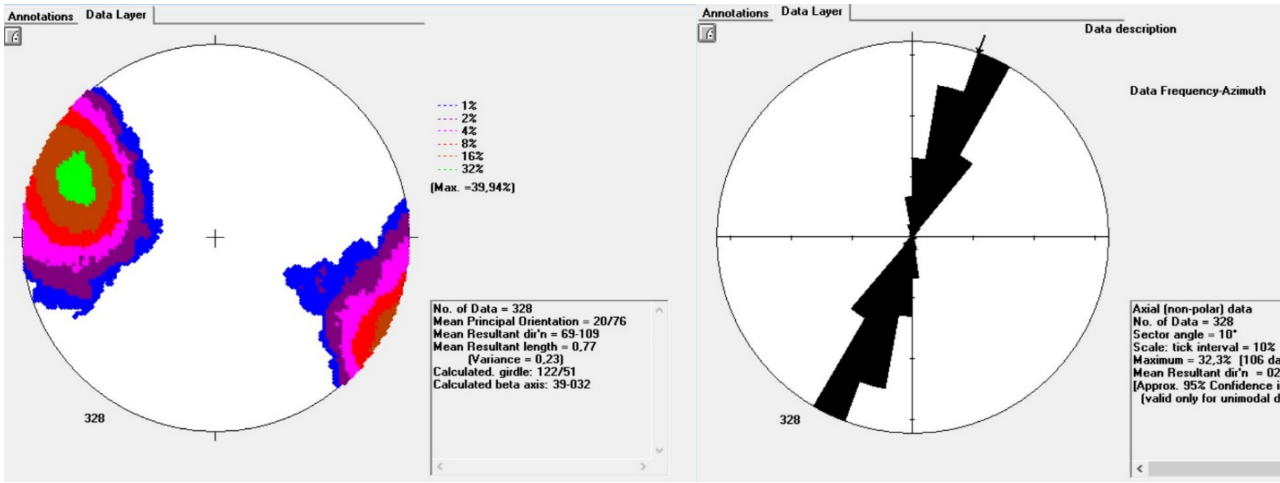

Figure 13. (a)Rose diagram of the Bedding (S0) N020/ 76 SE with secondarily towards NW; (b) Representation of polars of the Bedding

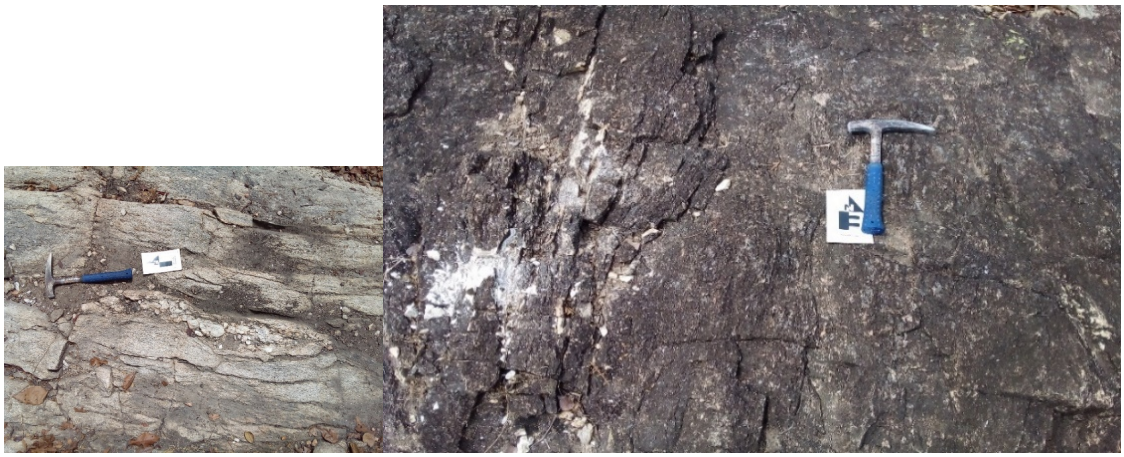

Figure 14. (a) shearing foliation S1 (N004/58 W) in an intense sinistral shear that marks the contact between batholith (granite) / Argillite; (b) Sinistral shearing S1(N024°/60 SE)

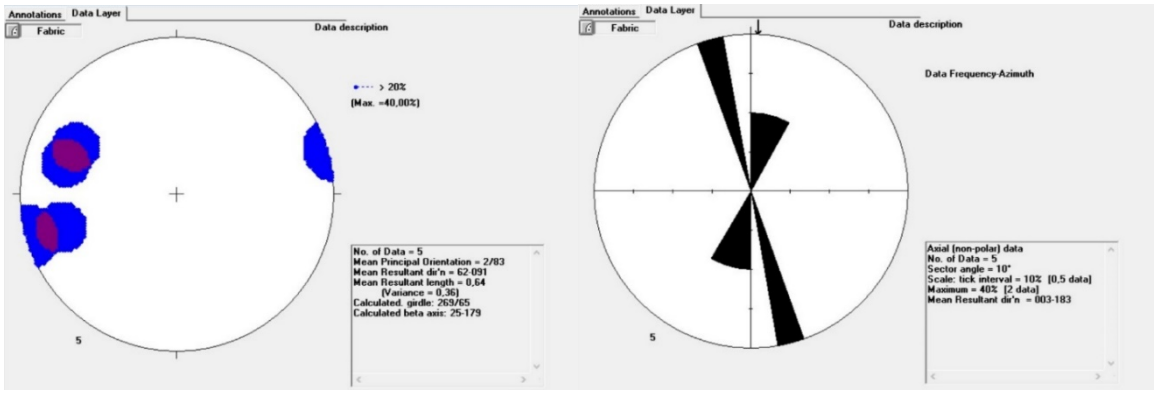

Figure 15: (a): Rose diagram of shearing foliation (S1) N003/ 83 E; (b): Representation of polars of the shearing foliation(S1)

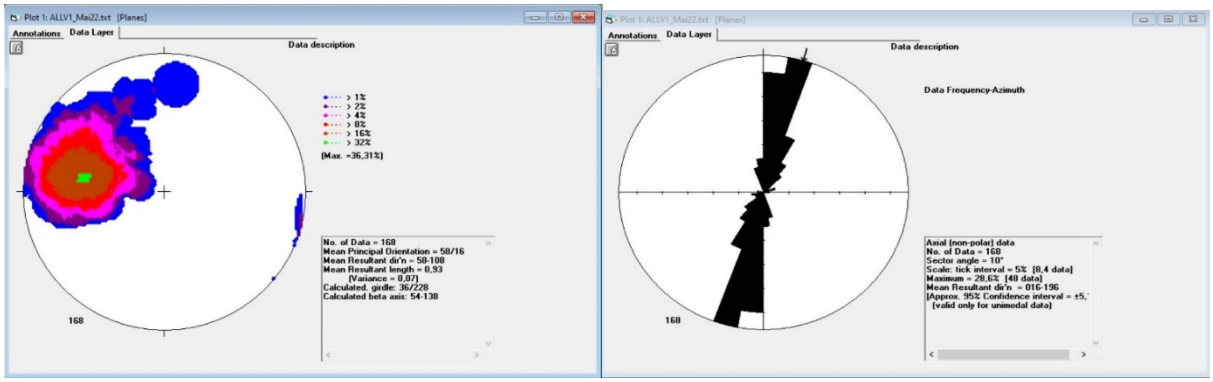

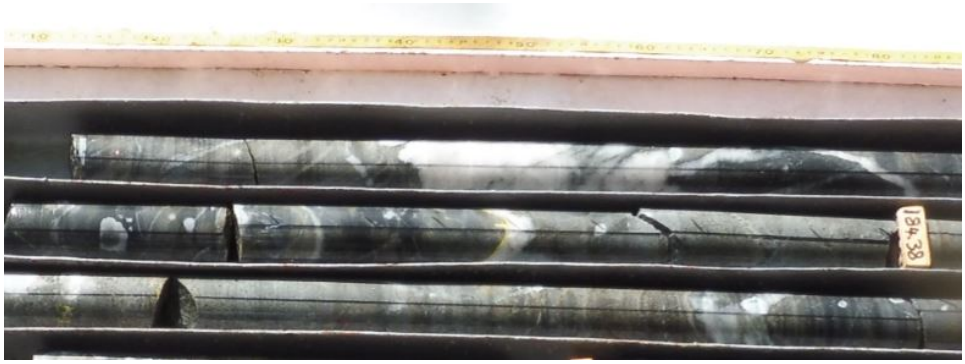

Figure 16. (a): Rose diagram of V1 quartz veins; (b): Representation of polars of quartz veins V1; (c): Quartz vein V1

Figure 17. . (a) Shearing foliation S2 (N000/ 54 E) which marks the shearing in the contact between the Tonalite / sandstone;

(b) Shearing foliation S2 (N000/ 54 E), metallograhic microscope

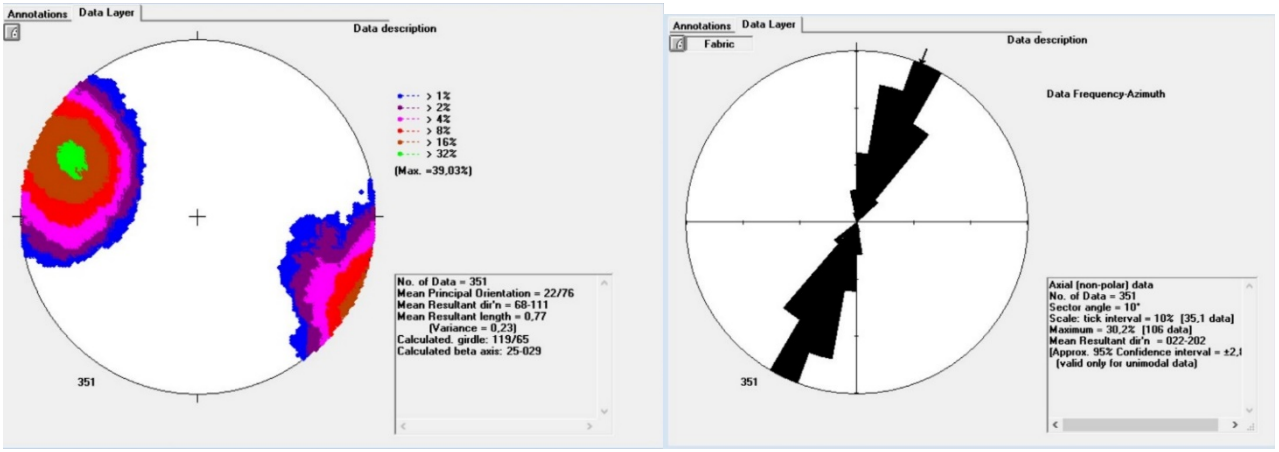

Figure 18. (a):Rose diagram of the Shearing foliation (S2) N022/ 76 SE; (b): Representation of polars of Shearing foliation S2

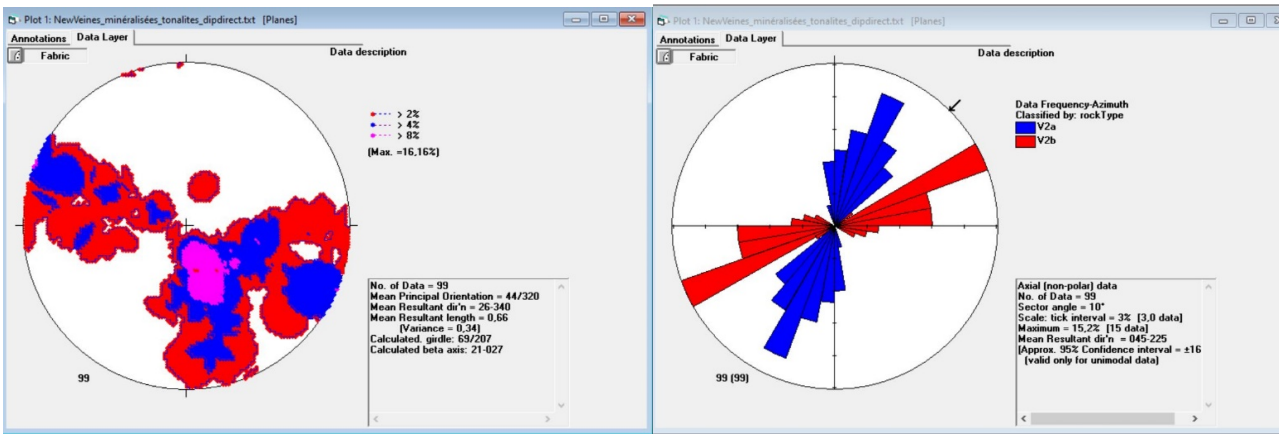

Figure 19. (a): Rose diagram of quartz veins V2a and V2b; (b): Representation of polars of quartz veins V2a and V2b

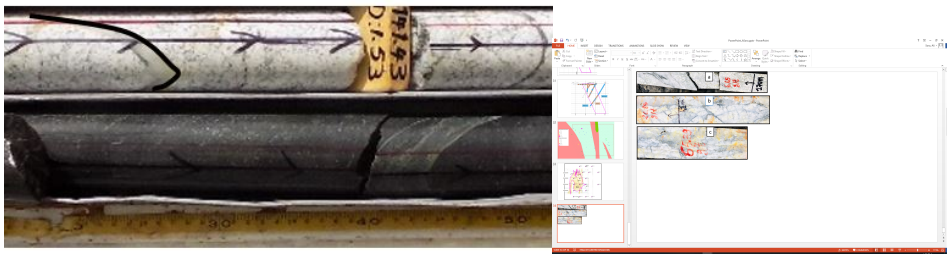

Figure 19. (c): V2a quartz vein; (d): Strongly mineralized quartz vein V2b (65.39 g/t)

4.2.2.3 Deformation D3

The D3 deformation is marked by diorite dykes that cut across the tonalite and metasediments. Diorite dykes were also identified and measured in core drill holes (Figure 20). The dykes strike N010 and dip 66° towards SE (Figure 21). The quartz veins associated with the D3 deformation are V3 veins. They are isolated and trends N044 and dips 85° towards the SE (Figure 22 a, b).

Figure 20: a: Photograh of diorite (TDY013) in drill hole FNDC008@103.3m, showing Shearing foliation S3, Contact Diorite / Sandstone b: Shearing filation S3 in (TDY013) in drill hole FNDC008@103.3m, metallograhic microscope

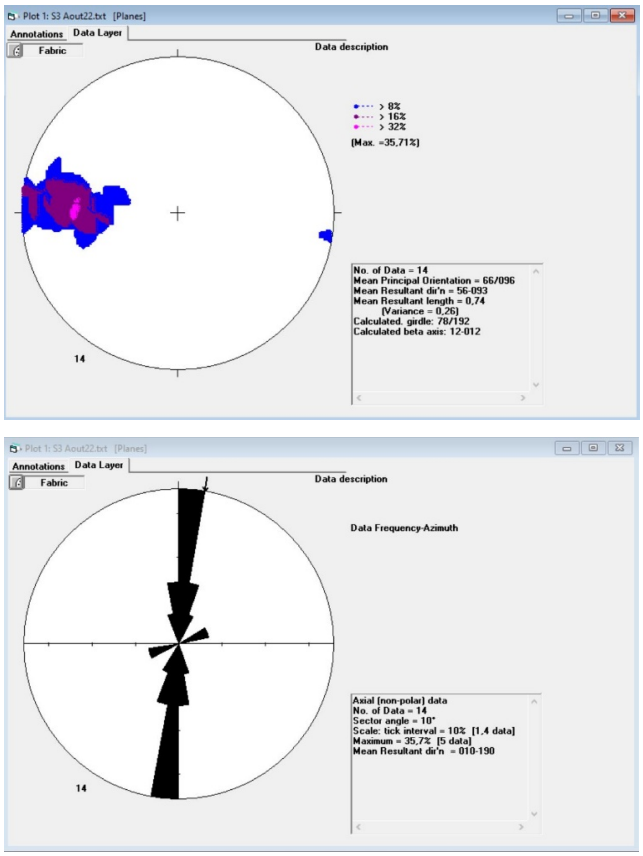

Figure 21. (a) Rose diagram of dyke planes (D3 deformation); (b) Representation of polars dyke

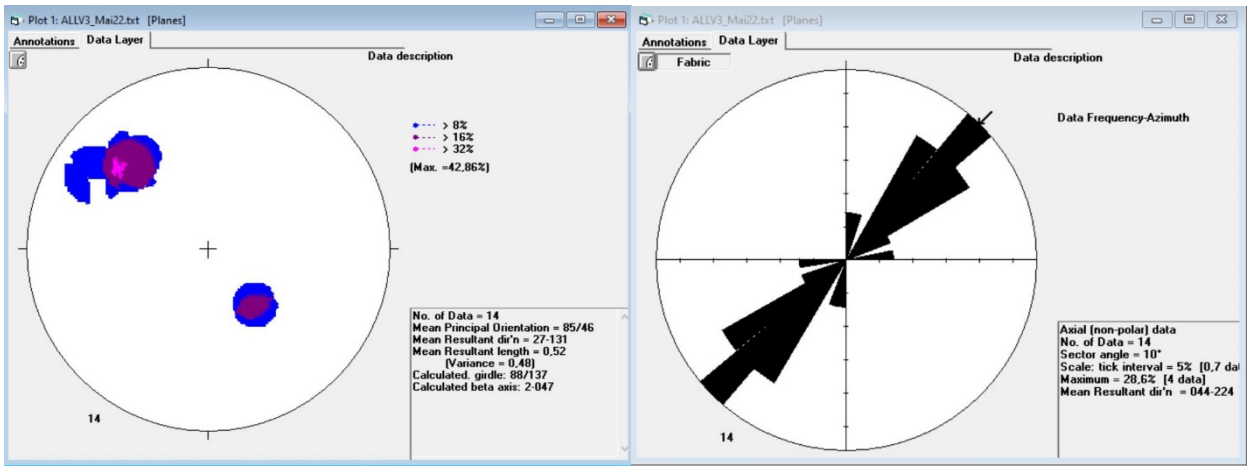

Figure 22. (a): Rose diagram of V3 quartz veins; (b): Representation of polars

of V3 quartz vein

5. VALIDATION

The main directions of the lineaments from the Landsat 8 image, Radarsat image and aeromagnetic image are four sets namely the directions N080-N100, N030-050, N000-N020, N120-N135. Relative to the data acquired in the field, we note the D1 deformation in the NS direction with strongly dipping towards east. The S2 shearing foliation of the D2 deformation has a NNE-SSW orientation and a strong dip towards SE then secondarily towards NW. These directions are respectively in phase with the directions N000-N020 and N030-050 coming from the lineaments. The quartz veins V2b associated with D2 deformation have a N070 -090 orientation and are in phase with the N080-N100 direction of the lineaments.

In conclusion, all lineaments identified from Landat 8, Radarsat and aeromagnetic images have been validated by field data except lineaments N120-N135. On the regional level, the first deformation D1 on the ground corresponds to the Eburnean deformation. The origin of the S1 foliation is discussed. Could it be linked to peribatholitic deformations [20]. On the ground, the S1 foliation transposes onto the S0 bedding. The S1 foliation is difficult to identify and is rarely observed in the field. The D2 regional event corresponds to a NW-SE shortening associated with the first major plutonic event which begins around 2160 Ma and gives numerous granitoid intrusions (Baratoux, and al., 2011), this corresponds to the S2 shearing foliation of the study area. The final phase of deformation corresponds to diorite dykes in the study area and is represented by D3. All these deformations have been represented, and an anticline and a syncline are interpreted in the study area.

The stereonet projections of these deformations shows that the dominant dip of the deformations is towards the SE (Figure 23 and 24) .

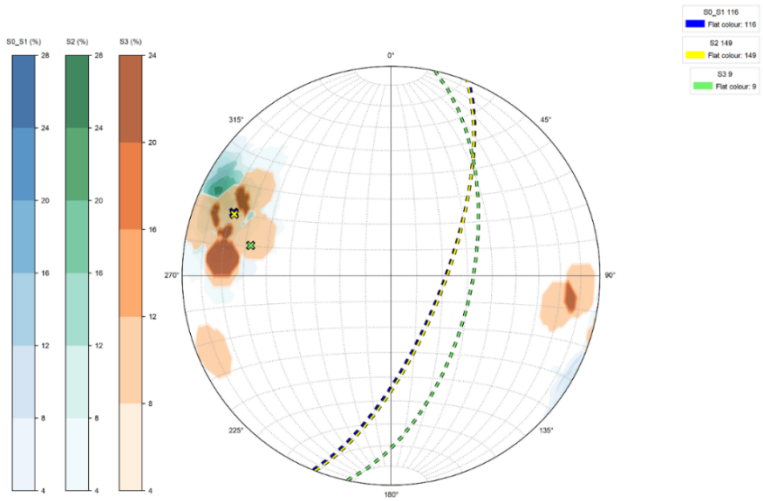

Figure 23. Stereonet projection of deformations (D1, D2, D3) from field dat

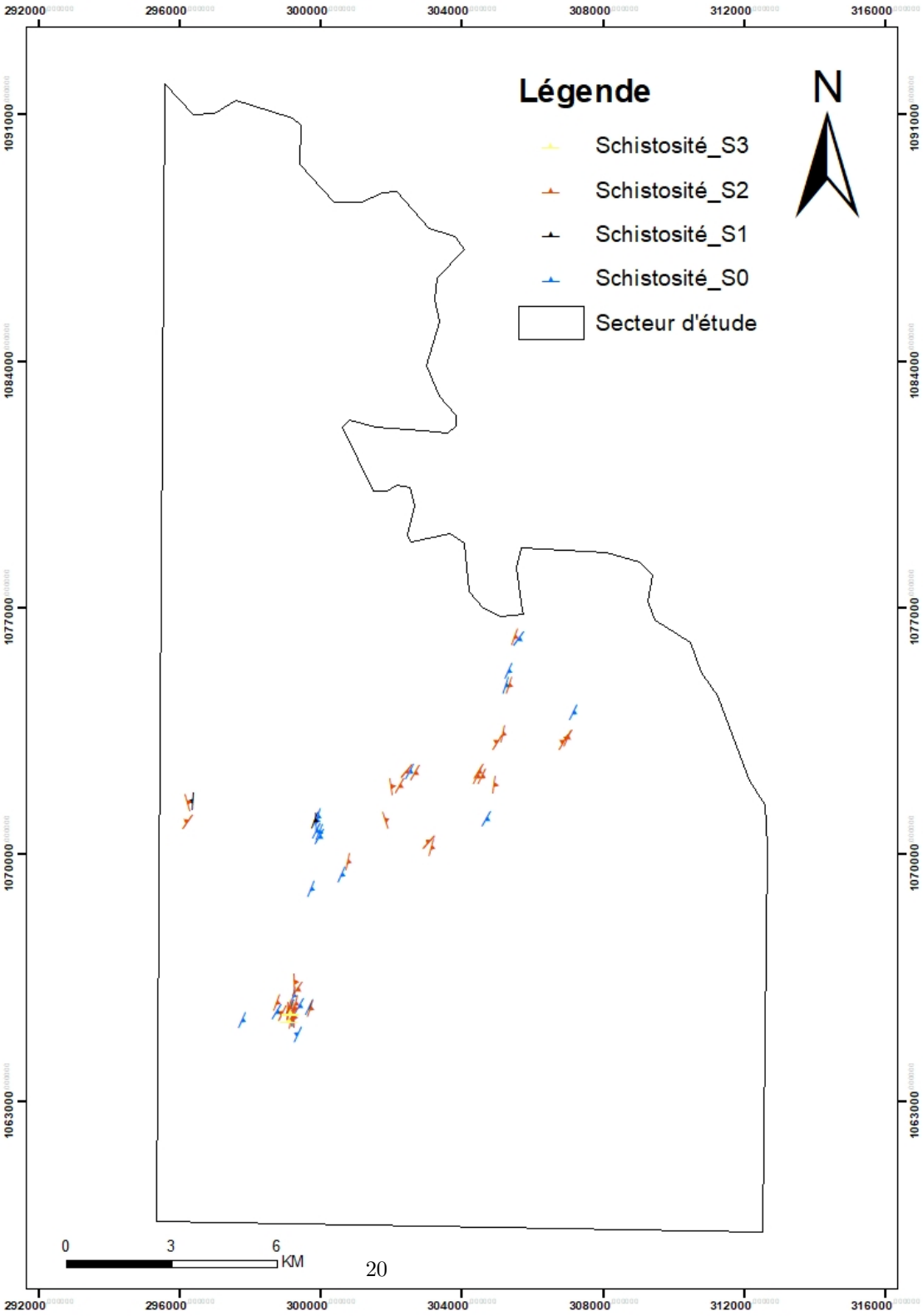
Légende
Schistosité_S3
Schistosité_S2
Schistosité_S1
Schistosité_S0
Secteur d'étude
N
0
3
6
KM
292000
296000
300000
304000
308000
312000
316000
1091000
1084000
1077000
1070000
1063000

Figure 24. Structural data map of the study area

6. STRUCTURAL CONTROL OF GOLD MINERALIZATION

Geochemical data have demonstrated that the most mineralized rock is tonalite. A study of the structures that are likely to trap gold in the tonalite has been carried out. According to the statistics made by the Leapfrog software, based on the five core drillings, it is the quartz veins V2b and fractures filled by sulphides then the veins V2a which host the highest gold grades in the tonalite, as indicated by the rose diagram. V2b mineralized strikes between N070 to N090 while V2a mineralized veins strikes N020 to N035. The average dip of all veins is 44° towards NW (Figure 25, 26 and 27). We were able to represent the different mineralized veins in the tonalite (Figure 28). This confirms that, it is the V2b quartz veins and then the V2a veins that carry the highest grades.

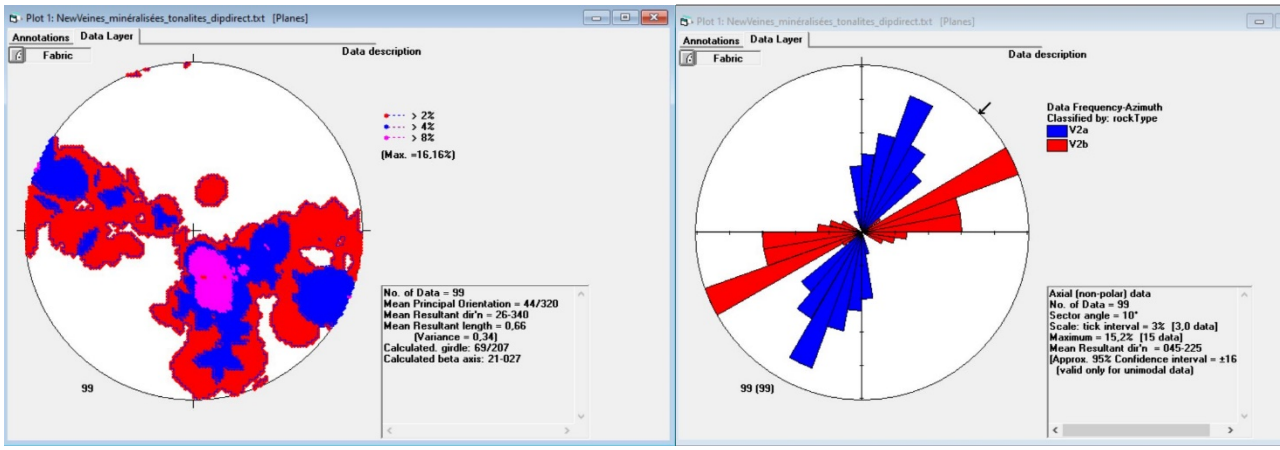

Figure 25. (a) : Rose diagram of all the quartz veins of the tonalite ; (b): Projections of polars of the quartz veins of the tonalite

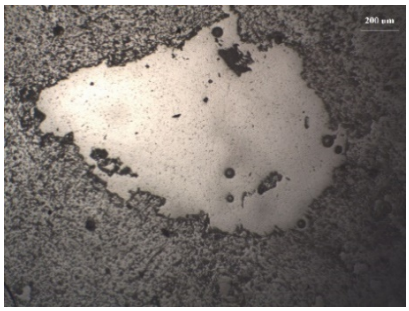

Figure 26. a: Smoky quartz vein (V2a) in tonalite with 26.82 g/t in core drilling hole FNDC012 (PDY005); b: Sulphide hosted in the Smokey Quartz Vein (V2a), metallographic microscope; c: quartz veinlet stockwork (V2b) in tonalite with 65 g/t in core drilling hole FNDC012@40.80m

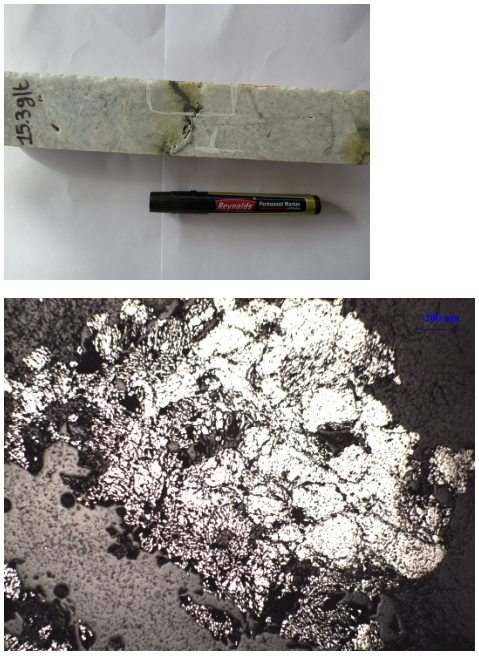

Figure 27. a: Fracture filled by sulphides in core drilling hole FNDC 008 (PDY 001); b: Sulfide in the fracture, metallographic microscope

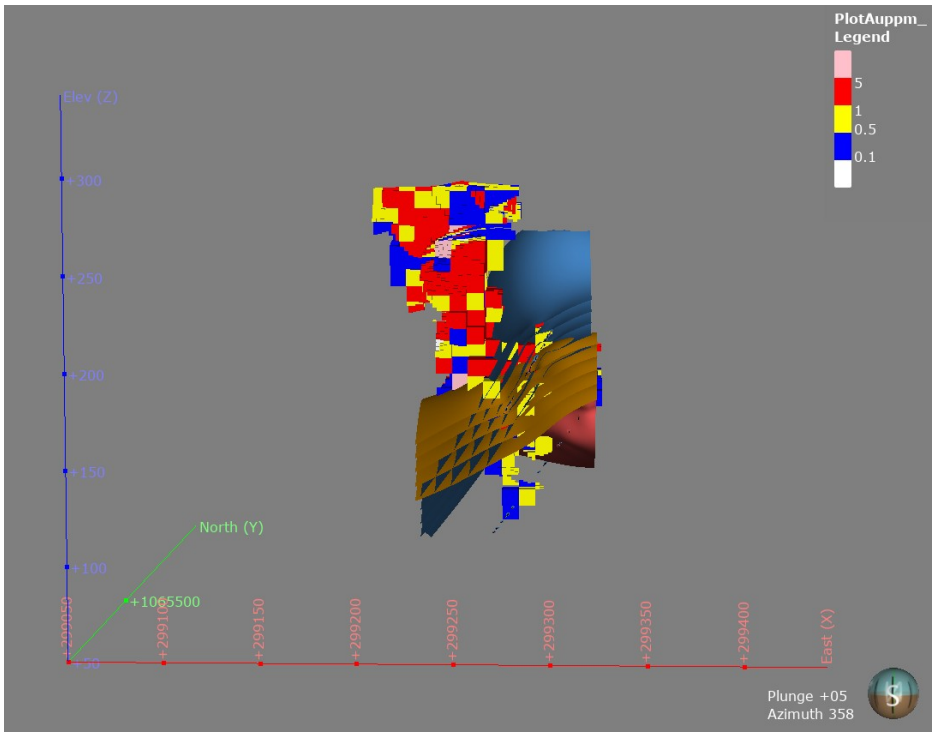

Figure 28. Representation of all quartz veins in tonalite envelope with grades

7. LITHOSTRATIGRAPHY OF THE STUDY AREA

In order to better understand the settng of gold mineralization, meticulous work has enabled the mapping of the Ouarigué prospect to be carried out.

The geology of this prospect is composed from west to east of argillite, tonalite, and sandstone. This tonalite is a small intrusion in the center, and we have the diorite dykes to the east. Then, a more precise block diagram was produced from the trench data and the drilling holes. Structural measurements were taken in order to characterize the mineralized structures. It follows a correlation of the structures coming from the trenches with those of the core drillings hole. This work made it possible to produce this block diagram which presents the different lithologies, the deformations D1, D2 and D3 (Figure 27) .

The lithostratigraphy of the study area is as follows: The setting of the metasedimentary basin on the basement is followed by bedding. Then, the D1 deformation appears and followed by regional metamorphism. Due to the position of the Ferkéssedougou batholith three kilometers west of the prospect, the D1 deformation is insignificant in the study area. Then, there is a tonalite intrusion which introduces the D2 deformation followed by the hydrothermal supply which leads mineralization. Finally, several diorite dykes (D3) intersects this

lithological setting and causes another gold mineralization.

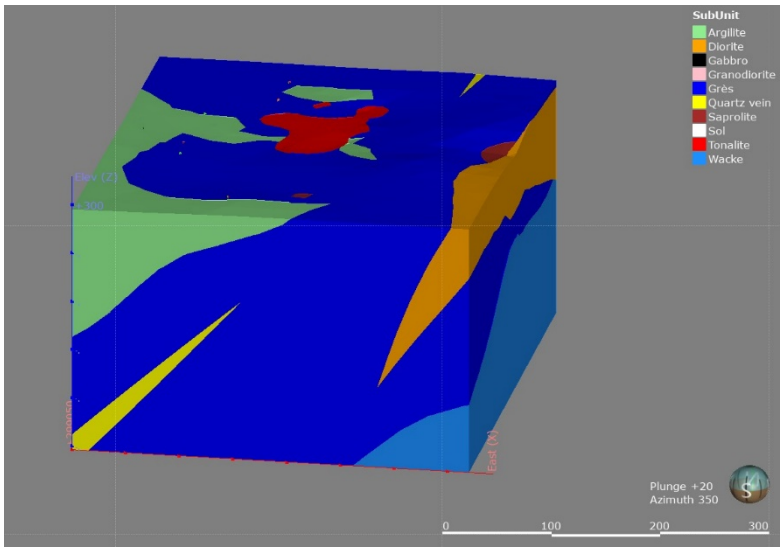

Figure 27. Block diagram of part of the study area

8. TYPE OF MINERALIZATION AND DISCUSSIONS

The study area has similarities with deposits in West Africa. According to Marwitz and al, 2016, there are three IRGS -type deposits in West Africa namely: the Morilla deposit in Mali , the Massawa deposit in Senegal and the Bonikro deposit in Ivory Coast. The Massawa orogenic deposit in Senegal arose from fluids that have a more magmatic origin according to Treloar et al, 2014. Indeed, the Morila mine has been qualified as an IRGS-type deposit by McFarlane et al., 2011. It is a deposit located in the south-east of Mali and hosted in greywackes and volcaniclastics . The mineralized structure is a NNE-SSW trending fold. Several intrusions of leucogranite , quartz diorite and finally muscovite-biotite granites have been identified on this deposit. (MacFarlane and al., 2011). Bonikro deposit was described by Ouattara et al, (2015) as being of the IRGS type in which the gold has a paragenesis Au + Mo+ S + W+ (Bi + Pb +Ag) in the granodiorite. The Bonikro mine located in the center of Côte d'Ivoire represents an IRGS-type deposit according to the work of Ouattara et al. 2015 (Ouattara and al., 2015). The mineralized rocks of this deposit consist of granodiorite with aplo-pegmatitic dykes with NS-oriented mineralized structures.

However, in the absence of mineralization dating data, the more general classification of Lang and Beker , 2001, was retained. There are three main types of mineralization related to hydrothermal alteration depending on the source of the hydrothermal fluid. Those are:

1) Mineralization linked to extrusive magmatism and volcanism, therefore to hydrothermal cells of seawater and meteoric water leading to the formation of auriferous volcanogenic massive sulphides and epithermal deposits;

2) Mineralization linked to crystallization and the liberation of magmatic fluids (porphyry, Intrusion - related gold system and skarn)

3) Mineralization related to fluids produced during deformation and metamorphism in deep zones of orogeny.

Our study area is of the second type, because it is linked to the crystallization of tonalite. The signature of gold deposits of the "Intrusion- related gold system –IRGS" type is: Au-Bi ±Te ±As ±Mo ±W (Baker, and al., 2001). This metallic signature is partly compatible with the signature of our study area which is Au-Te ±Bi ±Mo± Pb± Re. The mineralization of our study area is therefore the IRGS type.

Conclusion

The lithostratiaphy of the study area consists of a complex basement of metasediments (argillite sandstone and wacke). Then appear the intrusion of the Ferkéssedougou granite, granodiorite and tonalite. Later, diorite dykes crosscut the metasedimentary and the tonalite. Gold mineralization exhibits two forms. Quartz veins control the highest gold grades hosted in tonalite and in contact with metasediment. This mineralization took place during the second phase of deformation characterized by the S2 shearing foliation NNE orientation with a strong dip generally towards the SE but also towards the NW. Finally, the mineralization is affected by the D3 deformation induced by diorite dykes, responsible for another gold mineralization.

References

Baker,T., Lang, J.R., (2001), Fluid inclusion characteristics of intrusionrelated gold mineralization , Tombstone-Tungsten magmatic belt , Yukon Territory , Canada: Mineralium Deposita , c. 36, p. 563–582. https://doi.org/10.1007/s001260100189

Baratoux, L., Metelka, V., Naba, S., Jessell, M., Grégoire, M., Ganne J. (2011). Juvenile Paleoproterozoic crust evolution during the Eburnean orogeny (2.2–2.0 Ga), western Burkina Faso. Precambrian Research, 191 p. https://doi.org/10.1016/j.precamres.2011.08.010

Bessoles, B. (1977). Géologie de l'Afrique: le Craton Ouest Africain. *Mém. BRGM,* France, 88*,* 403 p.

Biémi, J., Deslandes S., Gwyn, H., Jourda, J.P. (1991). Influence des linéaments sur la productivité des forages dans le bassin versant de la Haute Marahoué (Côte d'Ivoire): Apport de la télédétection et d'un Système d'Information à Référence Spatiale". p. 43-49 in Gagnon, P. (éd). Télédétection et gestion

des ressources. Vol VII. Comptes rendus du septième congrès de l'Association Québécoise de Télédétection, 714 p.

Boher M., Abouchami W., Michard A., Albarède F., Arndt N. T. (1992). Crustal growth in West Africa at 2,1 Ga. Journal of Geophysical Research 97, n° B1, 345-369.

Djemai, S., Bendaoud, A., H, Haddum., Ouzegane, K., and Kienast, J. R. (2009). Apport des images Landsat 7 ETM+ pour la cartographie géologique des terrains archéens en zone aride : Exemple du terrane de l'In Ouzzal (Hoggar occidentale, Algerie). IIIèmes Journées d'Animation Scientifique du réseau de Télédétection de l'AUF JAS'09, Sous le thème : «Imagerie Satellitaire Multisources : Approches Méthodologiques et Applications», Alger, 8-11 novembre 2009.

El Gout, R., Khattach, D., Houari, M.-R. (2009). Etude gravimétrique du flanc nord des Béni Snassen (Maroc nord-oriental): implications structurales et hydrogéologiques. Bull Sci 61–75.

Himyari, S.M., Hoepffner, C., Benzakour, M., and Hadani D.E. (2002). Etude structurale du haut atlas oriental Maroc à l'aide de l'analyse linéamentaire des images HRV XS de Spot, Revue Télédétection, vol. 02, n°. 4, pp. 243-253.

Jourda, J.P., E.V. Djagoua, K. Kouamé, M.B. Saley, C.C. Gronayes, J.-J. Achy, J. Biémi and M. Razack. (2006). Identification et cartographie des unités lithologiques et des accidents structuraux majeurs du département de korhogo (nord de la côte d'ivoire): Apport de l'imagerie etm+ de landsat. Revue Télédétection, 6(2): 123- 142.

Kouamé, K.F., Lasm, T., Saley, M.B., Tonyé, E., Bernier, M., and Wade, S. (2009). Extraction linéamentaire par morphologie mathématique sur une image RSO de RadarSat-1 : application au socle Archéen de la Côte d'Ivoire," IIIèmes Journées d'Animation Scientifique du réseau de Télédétection de l'AUF JAS'09, Sous le thème : «Imagerie Satellitaire Multisources : Approches Méthodologiques et Applications», Alger, 8-11 novembre 2009.

Khattach, J.A.D. (2010). Contribution de la gravimétrie à l'étude de la structure des Hauts Plateaux (Maroc oriental). Bull. L'Institut Sci. Rabat 19–30.

Lopez, A., Nezry, E., Touzi R., Laur, H. (1992). Structure detection and statistical adaptive speckle filtering in SAR image. International Journal of Remote Sensing , vol. 14, no. 9, p. 1735-1758. https://doi.org/10.1080/01431169308953999

Masurel, Q. (2015). 4D evolution of the Sadiola-Yatela gold district, Kédougou-Kénieba inlier, West Africa. Ph.D. Thesis, The University of Western Australia, 238 p.

McFarlane, C.R.M., Mavrogenes, J., Lentz, D., King, K., Allibone, A., Holcombe, R. (2011). Geology and Intrusion -related affinity of the Morila Gold

Mine, southeast Mali. economic Geology , 106, 727–750. https://doi.org/10.2113/econgeo.106.5.727

Milesi, J.P., Feybesse, J.L., Ledru, P., Dommanget, H.A.S., Ouedraogo, M.F., Marcoux, E., Prost, A., Vinchon, C., Sylvain, J.P., Johan, V., Tegyey, M., Calvez, J.Y & Lagny P. (1989). The gold mineralizations of West Africa, their relations with the lithostructural evolution of the Lower Proterozoic. Chrono. Search _ Min., Fr.497, 98p.1. https://doi.org/10.1016/0301-9268(92)90123-6

Nezry, E., Lopez, A and Touzi, R. (1991). Detection of structural and textural features for SAR images filtering. in proceeding of IGARSS 91, pp. 2169-2172.

Ouattara, G. (1998). Structure du batholite de Ferkéssedougou (secteur de Zuénoula, Côte d'Ivoire). Implication sur l'interprétation de la géodynamique du paléoprotérozoïque de l'Afrique de l'ouest à 2,1 Ga. Thèse de doctorat. Univ. Orléans, 290 p.

Ouattara, Z. (2015). Caractères lithostratigraphiqie, structural, géochimique et métallogénique du gisement d'or de Bonikro, sillon birimien de Fettekro, centre-sud de la Côte d'Ivoire. Doct. Univ. Félix Houphouët-Boigny, Abidjan, 256 p.

Sonnendrucker, P. (1969). Etude de synthèse sur l'or en Côte d'Ivoire, rapport de fin de mission, SODEMI, Abidjan, rapport n°222, 127 p.

Ta, M.Y., T. Lasm, J.P. Jourda, F.K. Kouamé and M. Razack. (2008). Cartographie des accidents géologiques par imagerie satellitaire landsat-7 etm+ et analyse des réseaux de fractures du socle précambrien de la région de bondoukou (nord-est de la côte d'ivoire). Revue Télédétection 2008 8(2): 119-135.

Tagini, B. (1971). Esquisse structurale de la Côte d'Ivoire. Essai géotechnique régional, Thèse de Doctorat Univ. Fac. Des Sci. Lausannne (Suisse), et, SODEMI, Abidjan, 302 p.

Touzi, R., Lopez, A., Bousquest, P. (1988). A statistical and geometrical edge detector for SAR images. IEEE Transactions on Geoscience , Remote Sensing , vol. 26, no. 6, p. 764-773. doi: 10.1109/36.7708

Treloar, P.J., Lawrence, D.M., Senghor, D., Boyce, A. & Harbidge, P. (2014). The Massawa gold deposit, Eastern Senegal, West Africa: an orogenic gold deposit sourced from magmatically derived fluids ? Geological Society, 27p. https://doi.org/10.1144/SP393.12

Vanié, L.T.A, Khattach, D & Houari, M.R. (2005). Apport des filtrages des anomalies gravimétriques à l'étude des structures profondes du Maroc oriental. Bull. L'Institut Sci. Rabat Sect. Sci. Terre 2005 N°27 29-4 12.

Vanié, L.T.A., Khattach, D., Houari, M.-R., Chourak, M., Corchete, V. (2006). Apport des filtrages des anomalies gravimétriques dans la détermination des accidents tectoniques majeurs de l'Anti-Atlas (Maroc), in: Actes Du 3ème Colloque Maghrébin de Géophysique Appliquée. pp. 23–30.

Vidal, M., Delor, C., Pouclet, A., Siméon, Y. & Alric, G. (1996). Evolution géodynamique de l'Afrique de l'Ouest entre 2.2 Ga et 2 Ga: le style "archéen" des ceintures vertes et des ensembles sédimentaires birimiens du nord-est de la Côte d'Ivoire. *Bull. Soc. géol, Fr.,* 167, *3:* 307-319.

WAXI, 2018. Geological map of the West African craton

Yao, B.D. (1998) Lithostratigraphie et pétrologie des formations birimiennes de Toumodi-Fettekro (Côte-d'Ivoire): implication pour l'évolution pour l'évolution crustale du Paléoprotéroïque du craton Ouest-Africain. Thèse doc., Univ. Orléans, 191 p.

Yace, I. (2002). Initiation à la géologie. L'exemple de la Côte d'Ivoire et de l'Afrique de l'Ouest. Ed. CEDA, 183 p.

Yésou, H., Pion, J.C., Besnus, Y., and Saint-Jean R. (1993). Amélioration des données SPOT pour la cartographie structurale en milieu tropical. Exemple de la région des chapeaux de fer de Pagala Togo), IIIèmes Journées Scientifiques du Réseau Télédétection UREF, Toulouse, 13-16 novembre 1990, pp. 143-164.